Design of effective heat transfer structures for performance maximization of a closed thermochemical energy storage reactor through topology optimization

Humbert, Gabriele; Sciacovelli, Adriano

DOI:
10.1016/j.applthermaleng.2023.122146

Document Version
Publisher's PDF, also known as Version of record

Citation for published version (Harvard):
Humbert, G & Sciacovelli, A 2024, 'Design of effective heat transfer structures for performance maximization of a closed thermochemical energy storage reactor through topology optimization', *Applied Thermal Engineering*, vol. 239, 122146. https://doi.org/10.1016/j.applthermaleng.2023.122146

Applied Thermal Engineering 239 (2024) 122146

Contents lists available at ScienceDirect

Applied Thermal Engineering

journal homepage: www.elsevier.com/locate/apthermeng

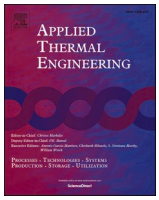

Research Paper

Design of effective heat transfer structures for performance maximization of a closed thermochemical energy storage reactor through topology optimization

Gabriele Humbert, Adriano Sciacovelli *

Birmingham Centre for Energy Storage, School of Chemical Engineering, University of Birmingham, UK

A B S T R A C T

This study addresses the need for heat transfer intensification in closed thermochemical energy storage reactors using topology optimization as a design approach. We introduce a novel topology optimization framework to simultaneously optimize fins geometry and amount of enhancer material while meeting specific discharge time, bed size, and bed porosity requirements. The proposed topology optimization framework is thoroughly tested by optimally designing innovative fin structures in a reference thermochemical storage reactor aimed at heat storage in industrial applications and operated with Strontium Bromide in the range 150-250 °C. The generated designs show performance improvement up to +286% compared to state-of-the-art designs. Our findings also indicate that the optimal amount of enhancer material varies significantly; large bed sizes with high packing factors maximize reactor energy density while highly packed reactive beds provide a larger amount of energy in fixed discharge times compared to less packed reactive beds. Finally, the benefits and limitations of the proposed topological optimization approach, as well as the extent to which the optimal designs found are generally applicable are thoroughly discussed to provide guidelines for configuring high-performing closed system thermochemical energy storage reactors.

1. Introduction

Thermochemical energy storage (TCS) systems present the advantages of high theoretical energy density, nearly negligible heat losses during the storage period and possible heat upgrading between charging and discharging steps [1,2]. In recent years, an increasing number of TCS prototypes have been tested for both domestic applications and industrial applications, and promising results have been published in the literature [3–5]. However, results consistently show that actual experimental performance remains far from the theoretical potential [3]. A crucial point that remains to be fully addressed is how to effectively configure TCS reactors in order to maximize the performance of TCS systems [6]. In particular, given the low thermal conductivity and low permeability of typical thermochemical materials (TCMs) [7], achieving effective heat and mass transfer in the reactive beds remains challenging. In the instance of closed system TCS systems, literature studies demonstrated that the heat transfer across the reactive bed is the main performance-limiting factor [8]. Therefore, enhancing heat transfer in reactive beds is crucial to increasing the amount of energy retrieved or delivered from TCS reactors in a given time, thus maximizing the overall system efficiency [9,10].

To enhance the thermal performance of TCS reactors, several studies have focused on heat transfer intensification by means of extended surfaces made of highly conducting material (HCM), such as aluminium, steel, or copper [11]. In the instance of a reactive bed employing Ca$(OH)_2$/CaO, Wang et al. [12] predicted and compared the thermal performance of three reactor architectures adopting extended surfaces. The results show that plate-pin fin sink reactors enhance the convective heat transfer in the reactive domain, ultimately leading to a dehydration time reduction of around -33% compared to plate-fin sink reactors. On the other hand, the hydration process is dominated by heat conduction mechanisms, and negligible performance differences were observed among the proposed reactor architectures. Similarly, Papakokkinos et al. [11] compared the thermal performance of five geometrical configurations for adsorption-packed bed reactors. Silica gel and water were considered as working pairs. For low bed porosity, i.e. highly packed TCM, a larger power density was predicted when honeycomb structures were adopted compared to radial fins. For high bed porosity instead, radial fins were found favourable. The design packing factor, defined as the ratio between the amount of metallic material over the total bed volume, was in the range from 0.16 to 0.41. More recently, Kant et al. [13] compared the performance of reactive beds utilizing variable fins geometry, concluding that using rectangular fins leads to superior performance. The size of the rectangular fins was optimized by means of surrogate models and an optimal design presenting a 0.10 packing factor

* Corresponding author.
E-mail address: a.sciacovelli@bham.ac.uk (A. Sciacovelli).

https://doi.org/10.1016/j.applthermaleng.2023.122146
Received 10 May 2023; Received in revised form 13 November 2023; Accepted 30 November 2023
Available online 5 December 2023

Nomenclature

Abbreviations

EOM	Energy output maximization
HCM	High Conducting Material
HTF	Heat Transfer Fluid
MUM	Material utilization maximization
TO	Topology Optimization
TCM	Thermochemical Material
TCS	Thermochemical Storage
PF	Packing factor

Symbols

c	Molar concentration [mol/m^3]
cp	Specific heat [J/kg/K]
$h(p)$	Pressure term [-]
h_{HTF}	Convective heat transfer coefficient [W/m^2/K]
h_{int}	Heat transfer coefficient at the HCM/TCM interface [W/m^2/K]
K	Permeability [m^2]
k_{cin}	Kinetic coefficient [1/s]
E	Discharged energy [kWh/ m^3]
$\dot{c}$	Reactants sink term [mol/ m^3/s]
M	Molar mass [kg/mol]
P	Thermal power [W]
p	Pressure [Pa]
p_{SIMP}	Material interpolation exponent for the SIMP scheme [-]
p_{TANH}	Material interpolation coefficient for the TANH scheme [-]
$\dot{q}$	Volumetric heat generation [W/m^3/s]
$\dot{q}_{int}$	Local heat flux at the materials interface [W/m^2/s]
R	Ideal gas constant [J/mol/K]
$r0$	HTF pipe outer radius [m]
T	Temperature [K]
t	Time [s]
t^*	Desired discharge time [s]
u	Velocity [m/s]
W	Reactive bed size [m]
$\boldsymbol{s}$	Design variable [-]
V^*	Maximum volume fraction [-]
ΔH	Standard enthalpy of reaction [J/mol]
Δs	Standard entropy of reaction [J/mol/K]

Greek symbols

Γ_{in}	HTF boundary [m^2]
Γ_{int}	HCM/TCM interface boundary [m^2]
Ω_D	Ground domain [-]
α	Reaction advancement [-]
β	Projection steepness parameter [-]
λ	Thermal conductivity [$W/m \bullet K$]
ρ	Density [kg/m^3]
γ	Stoichiometric coefficient [.mol/mol]
ε	Porosity [-]
μ	Dynamic viscosity [Pa·s]

Subscripts

TCM,0	De-hydrated state
TCM,1	Hydrated state
b	bed
r	reactor
eq	Equilibrium
s	Salt grains
v	Vapour

was obtained. Kant et al. [14] also investigated and optimized constructal fins for a building-integrated TCS system, studying the influence of design parameters (number of bifurcations, angles, length rations), concluding that optimized system has the potential to achieve energy storage density $>$ 80kWh/m^3 and costs less than 15 $/kWh. Nonetheless, the investigation was carried out through conventional parametric optimization, thus with a-priori decision on which design parameters, and thus which group of geometries, to be explored during the analysis [14].

A similar approach, in combination with principles of the Constructal law, has been pursued by Lorente and co-workers in a series of studies aimed at the optimization of TCS systems [15–17]. The results of such thermodynamic analysis revealed relationships between performances and main parameters describing the TCS reactor geometry. For instance, the effect of height, width and number of layers in the proposed fishbone structure [17], the effect of number of salt layers [15], and the effect of shape ratios [16] were considered. Although based on the application of Constructal law, the studies require a-priori decisions on what design parameters to consider in the analysis and thus also those to exclude, therefore necessitating a prior heuristic understanding from the analyst of what suitable geometry should be adopted and parametrized for the subsequent optimization. Studies suggest that relying on expert decisions based on parametric optimization may have certain limitations for the so-called design space, preventing to identify novel designs beyond those already implicitly defined through the expert decisions [18,19].

The performance enhancement delivered by annular and longitudinal fins was also investigated by Golparvar et al. [20] by means of three-dimensional modelling. The fins' height and spacing were varied to identify the optimal configurations. Overall, reducing the fins spacing decreased the coefficient of performance while increasing the specific cooling power. A 10% higher total cooling power was indeed predicted. However, as a side-effect, the reduction in fins spacing also caused undesirable re-sorption of material particles located in the regions of the system with lower temperatures. The results showed that annular finned tubes outperformed longitudinal ones for similar dimensions and operating conditions. In addition, the authors estimated using optimized configurations to save about 370 L of fuel per annum, with a consequent decrease in greenhouse emissions of 738 kg_{CO2}. Longitudinal fins were also investigated by Fernandes et al. [21]. In such a study, a final configuration with 27 internal fins and 120 external annular fins was predicted to produce a heat output 2.3 times larger than a finless adsorber. Also, long and slender units adopting a larger number of thin fins were indicated as favourable to enhancing the system performance. In a follow-up study [22], a 16% savings in the annual backup of thermal energy compared to a conventional storage system was predicted.

1.1. Originality and novelty of this work

Overall, from the studies discussed above, it is evident that the optimality of the extended surface designs varies depending on the system requirements and constraints. Further, despite the performance improvement achieved by the designs of extended surfaces proposed so far, such designs were limited to either traditional heat exchanger arrangements or those heuristically proposed by the investigators [14,16,23]. That is, the range of feasible designs was a priori suggested and subsequently studied through numerical methods to assess the effects of design modifications on the reactor performance. As a result, the obtained performance enhancement depended on the geometrical configurations initially conceived by the analysts and, thus, on the analyst's insights regarding the investigated physical problem.

To overcome these limitations, this work proposes and investigates

topology optimization to identify novel configurations that could enhance heat transfer and performance of TCS reactors. The present work goes beyond those on traditional parametric optimization methods [14,15,17] by means of topological optimization methods that do not require a priori definition and parametrization of geometrical features. Besides, the topology optimization approach adopted in this work is capable of systematically addressing design optimization for intrinsically time-dependent problems. The generated optimal designs, indeed, target objective functions that depend on the time-history of the system.

Topology Optimization (TO) is a form-finding methodology characterized by significant design freedom [24]. No initial design guesses are required, and the design is free to evolve towards its optimal configuration along with the optimization iterations. TO is, therefore, a generative design approach [25]. Meaning that it provides a paradigm shift for what concerns the specific roles of the analyst as well as of the optimization methodology. In particular, by being a generative design approach, the role TO (i.e. of the methodology) is to generate designs with the minimum number of constraints imposed and to 'offer' such designs to the analyst. The generation of this design is driven by both the TO algorithm and the physical model representing the investigated problem. The role of the analyst is then, by and large, to interpret the designs offered by TO methodology and to ascertain the causal reasons that made emerging the designs generated under the given constraints considered. This stands in marked contrast to traditional approaches, such as parametric optimization analyses [6,11,26], where the analyst generates the potential design configurations in the first place and specifies a restricted number of design parameters, whose optimal values are subsequently determined.

As thoroughly discussed in the paper, the proposed topological optimization approach allows to identify novel TCS reactor designs with significantly higher performance than those proposed so far. The work specifically focuses on a closed-type TCS system that has been proposed for industrial applications and that requires TCS reactors explicitly designed to achieve high heat transfer performance. TO has already been employed to maximize the performance of TES devices in the instances of sensible heat storage devices [27] and latent heat thermal energy storage devices [19,28,29]. However, only partial attempts have been made in the context of closed system thermochemical energy storage reactors [30]. In one of our previous studies, the performance of open-system TCS reactors was maximized by means of the topology optimization algorithm [18]. The study aimed at identifying optimal flow channel geometry to enhance mass transfer. However, closed system reactors, which are the focus of this paper, differ from open-system ones in terms of (i) the main limiting transfer mechanism, (ii) types of enhancer materials adopted, (iii) governing equations describing the reactor behavior [31] and (iv) optimized geometries.

To this date, no comprehensive topological design optimization and comprehension of associated effects on the performance of closed system TCS reactors has been made. Thus the understanding of the benefits and limitations of topology optimization method for closed system TCS is so far limited. The present paper rectifies such shortcomings of the existing body of literature through the following novel contributions:

1. A novel framework for topological optimization of heat transfer enhancement structures in closed-type TCS reactors.
2. Innovative designs of heat transfer enhancement structures obtained by applying the topology optimization framework to the reference closed-type TCS reactor.
3. Robust understanding of the benefits and potential limitations of topology optimization for closed-type TCS reactors.

Additionally, and uniquely to this work, the novel TO approach simultaneously provides optimal designs of heat transfer enhancement structures and optimal TCS reactor packing factor, thus answering two crucial design questions at the same time. Further, the design trends for the optimal designs and optimal packing factor of the TCS system investigated in this work are analyzed considering variable desired discharge times, bed size and porosity. Ultimately, this work explores the use of topology optimization as an alternative and novel design tool to identify TCS reactor designs that largely outperform the state-of-the-art. The benefits, limitations, and design guidelines emerging from the results and the proposed TO frameworks are extensively discussed.

2. TCS reactor configuration

A reference closed-type TCS system commonly adopted in the literature was considered in this work. The TCS system is depicted in Fig. 1; it is constituted of multiple TCS reactors, each one positioned inside a shell served with vapour through an evaporator/condenser component. The design is typical of closed systems and such modular configuration has been considered in a growing number of published works. The system is aimed at industrial applications such as heat recovery, and industrial batch processes which require reactor concepts explicitly designed for high specific thermal power and short discharge times [5,32]. The reference TCS system with its intended applications is therefore an ideal case for pursuing designs of high-performance heat transfer enhancement structures by means of TO.

Each reactor of the TCS system has a hexagonal cross-section with a heat transfer fluid (HTF) pipeline positioned at the centre of the reactor. The arrangement of TCS reactors with hexagonal cross-section shown in Fig. 1 allows for a ≈10% increase in storage material volume compared to circular cross-sections, i.e. cylindrical TCS reactors. Each TCS reactor is assumed to operate in an identical manner within the whole TCS system to operate under identical conditions. Under such assumptions, it is therefore sufficient to analyze and optimize only one of the reactors to address performance enhancement of TCS the whole system. The assumption has been widely adopted in the literature and prior studies demonstrated that it leads to sufficiently accurate numerical results in comparison to experimental measurements [5,6,33].

Strontium bromide is considered as the reference TCM, as also done in prior work on the whole TCS system [3,5]. As reported by Richter et al. [34], the hydration and dehydration of strontium bromide from/to mono-hydrate state have been identified as a potential reversible reaction for temperature ranges above 150 °C:

$$SrBr_2 + 1H_2O \leftrightarrow SrBr_2 \bullet 1H_2O + \Delta H_r^0 \tag{2.1}$$

the reaction provides a high specific energy storage density (291 kJ/kg) and thus a manner to thermochemically store heat for the intended industrial applications of the TCS system shown in Fig. 1. Additionally, strontium bromide has been employed and tested in a growing number of TCS reactors demonstrators with longitudinal fins [32,33], thus making SrBr2 a relevant choice for what concerns the development of both TCS technology as well as of the topology optimization framework.

The material properties of the monohydrated and dehydrated $SrBr_2$ are based on literature data and are reported in Table 1 [33]. The reported TCM thermal conductivity, λ_{TCM}, refers to the effective conductivity of the bulk. Thermal oil is used as a Heat Transfer Fluid (HTF) [5], while aluminium is selected as HCM, with its thermo-physical properties shown in Table 2. Reference dimensions considered for the TCS reactor are presented and discussed in Section 3.2

3. Numerical model and optimization approach

3.1. Optimization Approach

The TO framework proposed and adopted in this work is summarized in Fig. 2. First, a design case is defined, and a representative unit of the TCS configuration is identified. The optimal distribution of HCM in the reactive bed is subsequently obtained by means of the topology optimization procedure. Due to its efficient implementation, a density-based approach was adopted to describe the material distribution during the

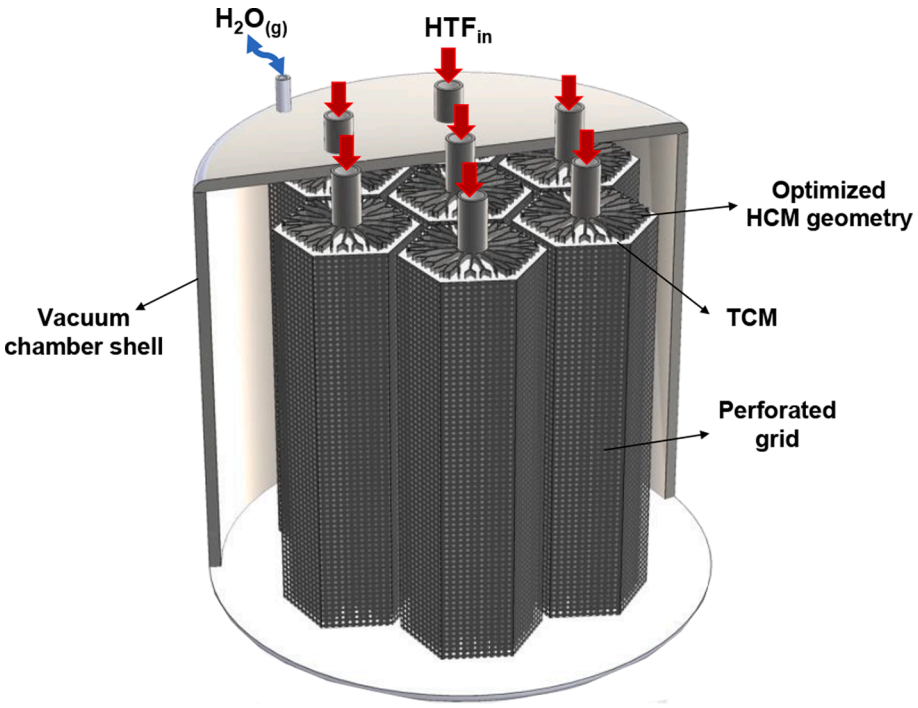

Fig. 1. Schematic of the TCS system configuration considered in this work.

Table 1
Thermophysical properties for $SrBr_2$ in anhydrous, subscript 0, and mono-hydrated, subscript 1, forms [31,33].

Property	Value	Unit
ΔH	71.98	kJ/mol_s
Δs	143.9	$J/mol_s/K$
γ	1	-
λ_s	1.0	W/m/K
$\varepsilon_{TCM,0}$	0.66	-
$\varepsilon_{TCM,1}$	0.71	-
$K_{TCM,0}$	10^{-10}	m^2
$K_{TCM,1}$	10^{-10}	m^2
$MW_{TCM,0}$	247	g/mol_s
$MW_{TCM,1}$	265	g/mol_s
$C_{p,TCM,0}$	305	J/kg/K
$C_{p,TCM,1}$	456	J/kg/K
$\rho_{TCM,0}$	4216	kg/m^3
$\rho_{TCM,1}$	3911	kg/m^3

Table 2
Thermo-physical properties for the selected HCM: aluminium [35].

Property	Value	Unit
λ_{HCM}	237	W/m/K
$c_{p,HCM}$	900	J/kg/K
ρ_{HCM}	2700	kg/m^3

TO procedure [36,37]. The density-based concept makes use of a continuous scalar indicator function for the tracking the materials involved in the problem [38], which in the present study are the TCM and the HCM. The indicator function, once discretized using a computational mesh, is commonly called s [28,39]. We follow such nomenclature in the present study. It is worthy to report a few key features of the indicator function for the benefit of the readership: firstly, $0 < s(\boldsymbol{x}) < 1 \forall \boldsymbol{x} \in \Omega$; that is, s takes a value between 0 and 1 *at each possible the position* $\boldsymbol{x}$ within the computational domain Ω over which topological optimization is performed. Secondly, within the context of the present work, $s = 1$ identifies the portion of the domain Ω occupied by the HCM. Conversely, $s = 0$ identifies the portion of the domain Ω occupied by the TCM.

The topology optimization framework proposed in this work (summarized in Fig. 2) allows to identify the optimal value of s *at each location within the computational domain*, and thus to determine the optimal topology of the HCM. That is, the optimal topology of the heat transfer enhancement structure within the TCS reactor. Therefore, s is the set of design variables that is optimized and it describes the topology of the TCS reactor. During each iteration, as illustrated in Fig. 2, the sensitivity of the target objective functions with respect to s is computed by solving the corresponding adjoint problem. The topology of the system, i.e. the design variable s, is then updated prior to re-solving the Finite Element (FE) model describing the transport phenomena describing the physical behaviour of the TCS reactor. The procedure is iterated until convergence is reached and optimal topology is identified. Further details about the formulation of the TO problem, objective functions definition, materials properties interpolation and algorithms employed are given in Section 3.

Because of using a density-based approach, interfaces between materials are not explicitly considered. In the context of the analyzed physical system, this apparently precludes the possibility of modelling interfacial thermal resistance between HCM and TCM, which in turn was observed to influence the reactor performance in recent studies from the literature [32,40]. Nevertheless, the approach proposed in this paper overcomes such limitations. Specifically, the generated TO designs were firstly reconstructed by means of CAD and then re-evaluated using the Finite Element (FE) model now accounting for the effect of the interfacial thermal resistance. Finally, the predicted performance was compared with a literature benchmark to assess the performance enhancement achieved by applying the whole methodology and workflow of Fig. 2. The whole TO framework was implemented by coupling COMSOL6.0 and MATLAB 2021, where COMSOL was used to perform the FE analysis while MATLAB was used to perform the steps specifically pertaining to topological optimization and to manage the workflow illustrated in Fig. 2.

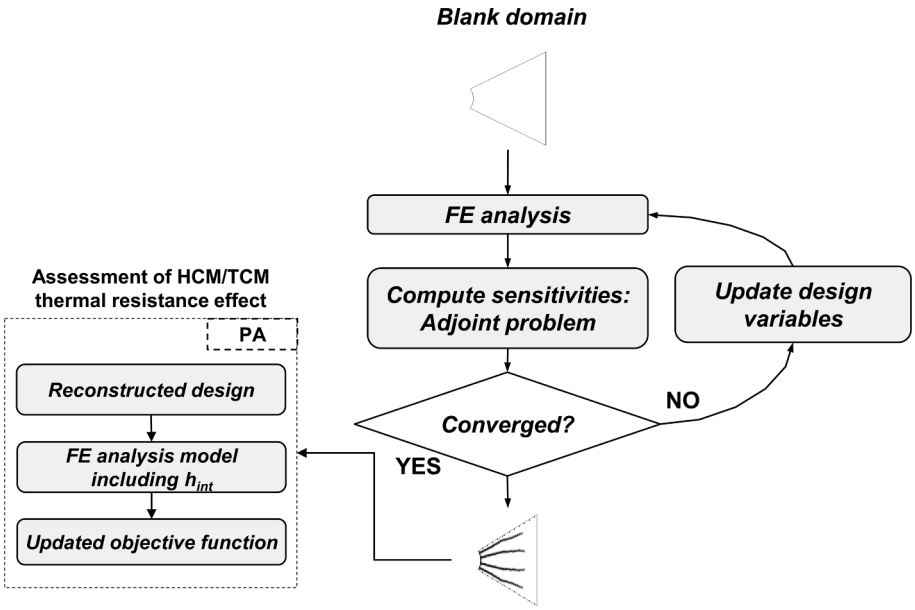

Fig. 2. Design approach for the heat transfer intensification in TCS reactors.

3.2. Governing equations

3.2.1. Computational domain and dimensions

As shown in Fig. 3, the computational domain considered in the present study consists of a two-dimensional representative cross-section of the TCS reactor. This choice allows to account for the analysis of the relevant transport processes (mass, energy) occurring along the *x-y* plane, while transport processes along the vertical direction of the reactor are neglected; Such two-dimensional modelling approach, widely adopted in the literature, has been proven to be accurate in comparison to experiments [5,6,33], and to allow accurate optimization of heat transfer enhancement structure [6,30]. Further, the symmetry of the cross-section was exploited, and only one-sixth of the hexagonal domain was investigated as a representative unit.

The relevant dimensions of the TCS reactor are labelled in Fig. 3 and reported in Table 3. Parameter *W* is the half distance between two adjacent HTF pipes; W is therefore the characteristic *cross-sectional dimension* of the reactive bed surrounding *a single* HTF pipe in the TCS system illustrated in Fig. 1. For the baseline TCS reactor design, a value of 50 mm was chosen for W. Such value was chosen in agreement with the dimensions of existing TCS reactor prototypes [5,33] to guarantee that the results obtained are representative and relevant. Nonetheless, cross-sectional dimensions of TCS reactors have been chosen in the literature across a wide range of values depending on the specific technical requirements for the TCS system. Therefore, two further values for W, i.e. W = 75 mm and W = 100 mm, were also considered to assess the effect of TCS cross-sectional dimension on the optimal HCM geometry. Section 4 thoroughly presents the corresponding results and discusses potential limitations in their applicability to TCS reactors with dimensions beyond those considered in the present study. Finally, referring to Fig. 3, r0 is the HTF pipe outer radius and it was chosen to be equal to 12 mm, which is in agreement with previous studies on closed system TCS reactors [26,41].

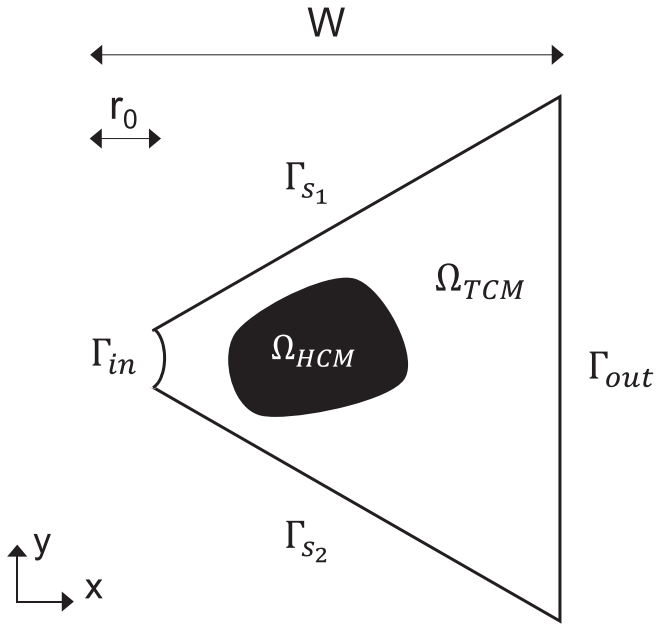

Fig. 3. Schematic of the domain considered for the heat transfer intensification of the TCS reactor.

3.2.2. Transport equations

The governing equations were expressed to allow for a density-based description of the distributed materials. The vapour mass balance was thus written in the following form:

$$\varepsilon(\boldsymbol{s})\frac{\partial c}{\partial t}+\mathbf{u}\nabla c=\dot{c}(\boldsymbol{s}) \tag{3.1}$$

where $\varepsilon(\boldsymbol{s})$ and $\dot{c}(\boldsymbol{s})$ are, respectively, the porosity and reactants sink terms; it is worthy to emphasize that both $(\boldsymbol{s})$ and $\dot{c}(\boldsymbol{s})$ are now design-dependent; that is, they depend on the topology described by $\boldsymbol{s}$. Further details on the topology-property relations are given in section 3.3.2.

Table 3
Main dimensions of the computational domain representative of the TCS reactor considered in this study.

Parameter	definition	Values	Unit	Ref
W	Half distance between two adjacent HTF pipes; main cross-sectional dimension of TCS reactor	50, 75, 100	mm	[26]
r_0	Outer radius of HTF pipe	12	mm	[41]

Inertial effects in the porous medium were neglected [42,43] in such a way that the velocity field, **u**, was assumed to follow the Darcy law:

$$\mathbf{u} = -\frac{K(s)}{\mu}\nabla p \tag{3.2}$$

with the term $K(s)$ indicating the design-dependent bed permeability and p representing the vapour pressure. Solid and gas phases were considered in thermal equilibrium [31,44], and, given the low vapour density in the porous medium [31,33], the convective heat transfer was neglected. This assumption is commonly adopted in the relevant TCS literature [26,31,42] and, as demonstrated in Section 3.2.3, sufficient to accurately predict the behaviour of TCS reactors. Thus, the energy conservation was written as:

$$\mathrm{C}(\mathbf{s})\frac{\partial \mathrm{T}}{\partial t} + \nabla \bullet (\lambda(\mathbf{s})\nabla T) = \dot{\mathrm{q}}(s) \tag{3.3}$$

where $\mathrm{C}(\mathbf{s})$ and $\lambda(\mathbf{s})$ refer to the design-dependent heat capacity and thermal conductivity, respectively. Finally, the reaction kinetics was written in the form [45] :

$$\dot{\alpha}(s) = k_{cin}(1-\alpha)\left(T_{eq,hydr}(p)[K] - T\,[K]\right)^{1.79} g(s) \tag{3.4}$$

where k_{cin} is the reaction kinetics term, while $g(s)$ is a design-dependent switch to activate the reaction kinetic equation only in the TCM regions. The equilibrium temperature was derived from the empirical correlation presented by Stengler et al. [46]:

$$log_{10}\left(p_{eq,hyd}[kPa]\right) = 8.18 - \frac{3.19*10^3}{T[K]} \tag{3.5}$$

the volumetric heat generation, $\dot{\mathrm{q}}(s)$, was calculated as a function of $\dot{\alpha}(s)$ according to equation (3.6):

$$\dot{q}(s) = \frac{(1-\varepsilon_0)}{M_{s,0}\rho_{s,0}}\dot{\alpha}(s)\Delta H g(s) \tag{3.6}$$

while the reactant sink term for the vapour mass conservation was calculated as:

$$\dot{m}(s) = -\frac{(1-\varepsilon_0)}{M_{s,0}\rho_{s,0}} M_v \dot{\alpha}(s) g(s) \tag{3.7}$$

the material interpolation strategies are detailed in section 3.3.2 and were formulated in such a way to recover the material properties in Ω_{HCM} and Ω_{TCM} and in accordance with the key definition of s:

$$s = \begin{cases} 0 \ in \ \Omega_{TCM} \\ 1 \ in \ \Omega_{HCM} \end{cases} \tag{3.8}$$

where Ω_{TCM} and Ω_{HCM} indicate the portions of the domain corresponding to the TCM and the HCM, respectively. Furthermore, the following equation is adopted to define the packing factor in the TCS reactor:

$$PF = \frac{\int_{\Omega_{HCM}} 1\, dxdy}{\int_{\Omega_d} 1\, dxdy} = \frac{V_{HCM}}{V_d} \tag{3.9}$$

where Ω_d is the ground domain, defined as $\Omega_d = \Omega_{TCM} \cup \Omega_{HCM}$. Thus the packing factor PF quantifies the fraction of the total domain Ω_d filled by the HCM. That is, the fraction of TCS reactor taken up by the heat transfer enhancement structure.

3.2.3. Boundary and operating conditions

Boundary conditions were chosen to replicate the typical conditions the TCS reactor is expected in the envisioned industrial applications outlined in Section 2 and for which the TCS reactor has been experimentally tested [5]. This choice ensures the TO results fit the specific application context for which TCS system illustrated in Fig. 1 has been conceived for. This study exclusively focused on hydration reactions. The significance of this choice lies in the crucial role of hydration for TCS applications. Hydration influences the discharging phase, dictating both the quantity of recoverable heat and the temperature at which it becomes accessible through a TCS system. In contrast, dehydration can be accelerated by elevated temperatures during the charging phase of the system, as reported in previous studies [31,40,47]. Referring to the computational domain shown in Fig. 3 and the mass transfer problem (Equation (3.1), a zero-mass flux condition was applied along the boundary Γ_{in} corresponding to the interface with the HTF pipe to model that no vapour flux takes place across the wall of the HTF pipes. A vapour pressure $p_{v,in}$ = 67 kPa was specified along boundary Γ_{out} by means of a Dirichlet boundary condition. The imposed value of vapour pressure along boundary Γ_{out} corresponds to the inlet vapour pressure of the TCS system (Fig. 1). This choice is consistent with modelling exclusively the representative TCS reactor cross-section (Fig. 3) and neglecting the effect of potential external structures (e.g. vapour distribution channels, vapour distribution mesh); the same approach was pursued in the literature [6,13,33] where high-fidelity numerical predictions were achieved. The specific value $p_{v,in}$ = 67 kPa was selected according to the experimental study of Sengler et al [5]. For what concern the energy transfer problem (Equation (3.3), a Robin boundary condition was applied along the boundary Γ_{in} corresponding to the interface with the HTF to model the transfer of heat between the HTF and the TCS reactor. A heat transfer coefficient h_{conv} = 1555 W/m^2/K and a HTF fluid temperature T_{HTF} of 207.6 °C were selected to replicate the same operating condition adopted by Sengler et al. [33]. The heat transfer coefficient value was derived from the Gnielinski empirical model for turbulent flow [48] assuming a HTF mass flow equal to 7.1 kg/min [33].

In summary, although TCS systems might be operated under different combinations of partial pressure and temperature [49], the boundary conditions used in this study are those representatives of the typical operating condition of TCS system being studied. Using such conditions ensures that the TO analysis is relevant to the specific intended applications of the TCS system being studied in this work. This, in turn, allows assessing the potential and benefit of the proposed topology optimization framework for TCS system, which is the primary focus and novelty of this study. Potential for future work on the influence of variable operating conditions on the topological optimization of TCS reactors is discussed in the final sections of this paper.

As the density-based approach does not allow for the explicit tracking of the material interfaces, the effect of interfacial thermal resistance was evaluated a posteriori on the reconstructed optimal designs. That is, for the optimal designs the interface between HCM and TCM was reconstructed and the FE model (governing equations in section 3.2.2) was re-solved now including the effect of the interfacial thermal resistance interface as follows:

$$\dot{q}_{int} = h_{int}(T_i - T_j) \tag{3.10}$$

where $\dot{q}_{int}$ is the local heat flux, T_i and T_j at the local domain temperatures at the interface, while h_{int} is the thermal resistance coefficient. Fig. 4 depicts a reconstructed design and the boundary Γ_{int} , namely the interface between HCM and TCM materials, where equation (3.10) was imposed.

The numerical model was validated in the instance of the hydration process of $SrBr_2 \bullet 1H_2O$. The data presented by Stengler et al. [33] were considered. In the study[33], Stengler et al. proposed a reactor design aimed at achieving high power density. The tested design presented radial fins with multiple branches. Notably, the design was not obtained employing any rigorous optimization algorithm, but rather generated in agreement with the heat transfer intensification guidelines from both topology optimization [36] and constructal theory [50]. Besides, in a follow-up study, Stengler et al. [33] modelled and calibrated the thermal resistance at the TCM/HCM interface as a function of the reaction advancement:

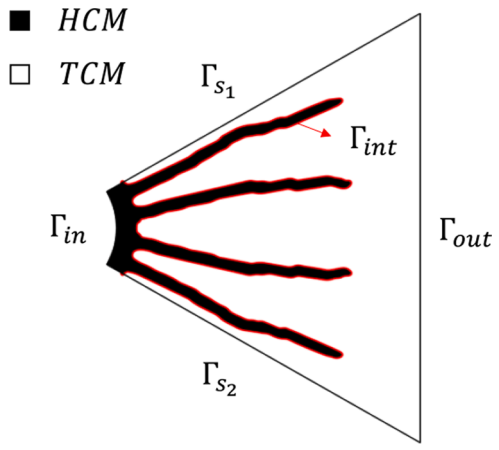

Fig. 4. Schematic of the domain and boundaries for a reconstructed optimal design.

$$h_{int} = 30 + 15\alpha \tag{3.11}$$

The same expression for the thermal resistance at the TCM/HCM interface was therefore also employed in the present work. Besides, The comparison between numerical predictions obtained with the model proposed in this study and experimental data from [33] is reported in Fig. 5(a), which shows the reaction advancement histories. An excellent agreement with the experimental data is observed when the thermal resistance coefficient, h_{int}, is considered. On the other hand, a larger reaction advancement rate is predicted by the TO framework when interfacial thermal resistance is not included, which in turn leads to an overestimation of the TCS reactor bed cooling. Fig. 5 (b) depicts instead the local temperature time evolution measured at the thermocouple B location, which was located at a 12 *mm* distance from the HTF pipe [33]. The qualitative evolution of the temperature over time is well reproduced by the FE model, although an overestimation of the maximum temperature values is observed. This is somehow expected since pointwise measurements, as the one shown in Fig. 5 (b), are affected by local non-homogeneous conditions not captured by the model, for example, non-homogeneous particle TCM particle size and uneven porosity of the TCS reactor bed. Nevertheless, as shown in Fig. 5 (b), the numerical framework used in this work is in good agreement with the predictions from the numerical model developed [33] once the interfacial thermal resistance is included. This allows us to conclude that the proposed numerical framework accurately reproduces state-of-the-art modeling of the TCS reactor and it is thus robust for the aims of the present work.

3.3. Topology Optimization

3.3.1. Problem formulations

Essential for TO is the problem formulation. That is the definition of the objective function and of optimization constraints that reflect the conditions the system under investigation is exposed to. Regarding the TCS reactor considered in this study, a rapid discharge of stored energy is desirable since the TCS reactor is intended for heat storage in industrial applications where the duration of the charge/discharge cycles is expected to be sub-daily [51]. Discharge times in the range 0.25 – 2h were considered in agreement with [33].

Discharge of maximum amount of energy in a fixed discharge time, or vice versa, discharge of fixed amount of energy in the least amount of time were considered in the TO problem formulation. Previous studies demonstrated such optimization problems to be equivalent [28], with the same optimal design emerging regardless of the considered objective function. Consequently, in this work, the maximization of the discharged energy in a fixed time was analyzed. Specifically, the following two optimization problems were formulated:

1) The material utilization maximization (MUM) problem. The MUM problem is summarized in the following way:

$$\begin{cases} max\, \alpha_{t^*} = \int_{\Omega_D} \alpha\,(\mathbf{s})\, dxdy \text{at t} = t^* \\ s.t. \int_{\Omega_D} \boldsymbol{s}\, d\boldsymbol{x} - V^* \leq 0 \\ 0 \leq s \leq 1 \end{cases} \tag{3.12}$$

which represents the maximization of the reaction advancement at the desired discharge time, t^*. The term V^* corresponds instead to the maximum prescribed packing factor PF. The resulting optimal designs present a final HCM/TCM volume fraction that coincides with the maximum value prescribed. The use of lower HCM/TCM volume fraction is not attractive for the optimizer, as this would imply larger TCM amounts and, thus, lower final reaction advancements. On the other hand, the use of a constraints-free optimization problem would lead to the trivial solution of a ground domain filled only with HCM, as this does not present any chemical energy content and thus 'maximizes' the final reaction advancement.

As expressed by equation (3.6)., the amount of heat generated during the reaction is proportional to the rate of reaction and, given the boundary conditions detailed in section 3.2.3, the heat generated from the reactive bed is entirely transferred to the heat transfer fluid. Consequently, the maximization of α_{t^*} is equivalent to the maximization of the energy discharged from a given amount of storage material. The MUM problem was formulated in agreement with the typical

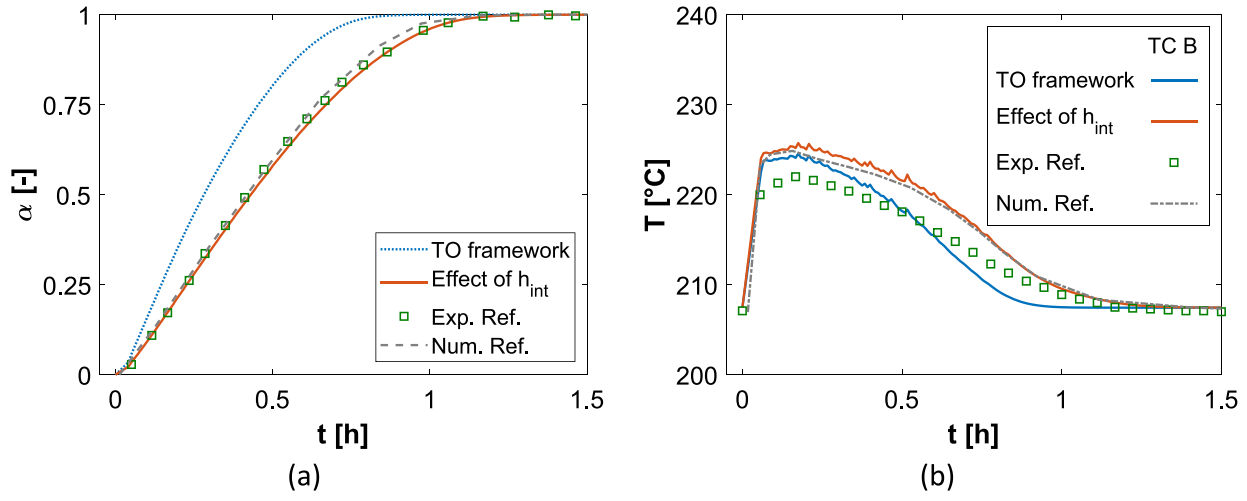

Fig. 5. Numerical model validation against literature data from [33]: (a) reaction advancement histories; (b) local temperature evolution in time for thermocouple B.

optimization problems adopted in the literature [19,28,30].

2) The energy output maximization (EOM) problem. The EOM is formalized in the following way:

$$\begin{cases} max\, E_{t^*} = \int_0^{t^*} \int_{\Omega_D} \frac{\dot{q}(\mathbf{s})}{V_d} dxdydt \\ s.t. \int_{\Omega_D} \boldsymbol{s}\, d\boldsymbol{x} - V^* \leq 0 \\ 0 \leq s \leq 1 \end{cases} \tag{3.13}$$

with E_{t^*} representing the amount of energy discharged from the reactive bed. It is worthy to emphasize that in the EOM problem the amount of HCM material is not strictly prescribed. In this sense, the EOM differs from the MUM since trivial optimal solutions cannot emerge. If no HCM is utilized, the rate of discharged energy might result too slow to achieve optimal performance. On the other hand, if no TCM is used, no net energy output is achieved. Between these two extreme cases the optimal solution for the EOM problem is expected to be found, and the optimization problem formulation does not require any additional constraints. Thus, the EOM problem allows to simultaneously obtain the optimal topology and the optimal packing factor. Nonetheless, a maximum threshold of $V^* = 0.4$ was considered in this work to avoid the generation of optimal designs with poor practical use due to predominant amount of HCM and limited amount of TCM.

Fig. 6 provides a simplified representation of the discharged energy and packing factor histories along the optimization iterations for both MUM and EOM problems. The packing factor, PF, value is defined as the ratio between the HCM and reactive bed volume, with V^* expressing the maximum packing factor value prescribed for the specific design problem. In MUM the the packing factor coincides with the prescribed V^*. Conversely, in the EOM, the packing factor is free to vary over the optimization iterations until its optimal value and optimal topology are found. Further, in Fig. 6 the maximum E_{t^*} represents the amount of chemical energy stored in the reactive bed and is linked to the reactor packing factor. While maximum E_{t^*} is fixed in the MUM problem, the packing factor value changes during the EOM problem iterations, and so does the maximum E_{t^*}. When convergence is reached in the EOM problem, the optimal packing factor value is found and thus also the corresponding E_{t^*}.

3.3.2. Material interpolation

The density-based topology optimization requires the interpolation of the material properties [24]. This is obtained using artificial laws describing the material properties' evolution as a function of $\boldsymbol{s}$. A crucial feature of such artificial laws is to make intermediate values unattractive so that final binary designs can be obtained from the optimization routine. In this work, the conventional SIMP interpolation method is used to interpolate the thermal conductivity term $\lambda(\mathbf{s})$ and for the heat capacity, $C(\mathbf{s})$:

$$\lambda(\boldsymbol{s}) = \lambda_{TCM} + (\lambda_{HCM} - \lambda_{TCM})\boldsymbol{s}^{p_{SIMP}} \tag{3.14}$$

$$C(\boldsymbol{s}) = C_{TCM} + (C_{HCM} - C_{TCM})\boldsymbol{s}^{p_{SIMP}} \tag{3.15}$$

where coefficient p_{SIMP} represents the penalization exponent. The thermal conductivity of the porous TCM is calculated as follows [15]:

$$\lambda_{TCM} = \lambda_s(1 - \varepsilon_{TCM}) + \lambda_v \varepsilon_{TCM} \tag{3.16}$$

Where λ_s is the thermal conductivity of the salt grains, while λ_v is the thermal conductivity of the water vapour. In order to achieve stronger penalizations, a TANH interpolation scheme was adopted for the permeability interpolation, with the material properties switch operated at $\boldsymbol{s} = 0.5$ [52]:

$$K(\boldsymbol{s}) = (1 - m_{TANH}(\boldsymbol{s}))K_{TCM} + m_{TANH}(\boldsymbol{s})K_{HCM} \tag{3.17}$$

with the design-dependent parameter $m_{TANH}(\mathbf{s})$ defined according to:

$$m_{TANH}(\boldsymbol{s}) = \frac{tanh\left[p_{TANH}(\boldsymbol{s} + sgn(k_{TCM} - k_{HCM}) \bullet 0.5 - 0.5) + 1\right]}{2} \tag{3.18}$$

with *sgn* denoting the sign function. As a result of the TANH scheme, the optimizer might allocate 'grey' material characterized by 'black' material properties, which is an undesired feature for the overall

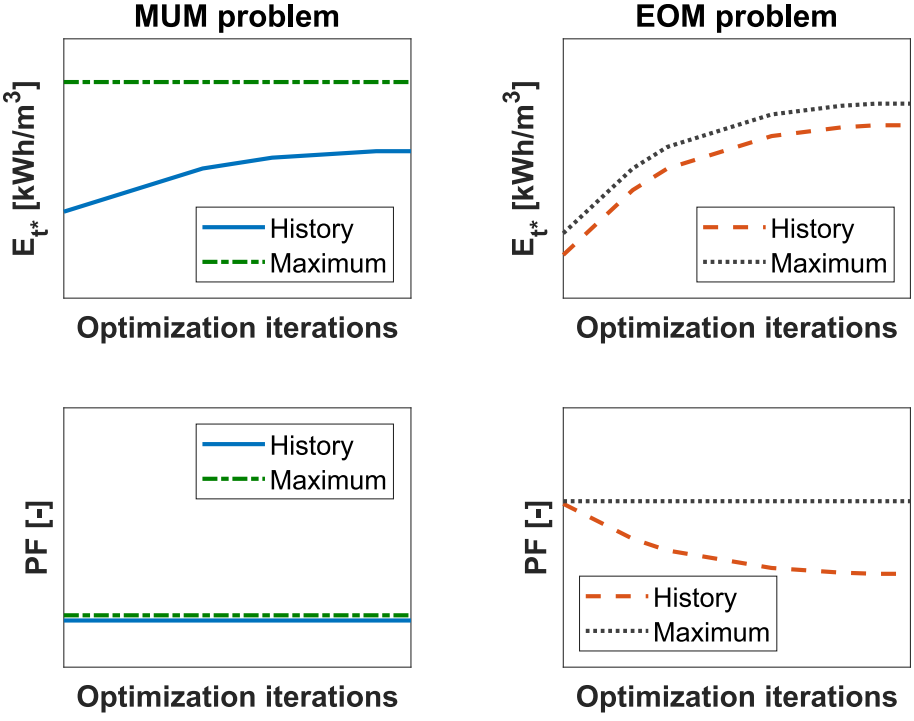

Fig. 6. Histories for discharged energy and packing factor for the material utilization maximization (MUM) problem and energy output maximization (EOM) problem.

optimization strategy. However, the combination of a TANH approach with a SIMP interpolation allows for the full material properties to be described only by large s values, thus still penalizing intermediate values. That is, the de-coupling of the material properties transitions precludes regions with intermediate properties for both permeability and e.g. thermal conductivity. Linear interpolation is adopted instead for the design-dependent switch $g(s)$, and for the bed porosity, $\varepsilon(s)$.

Filtering and regularization techniques are adopted to ensure the results' mesh-independence and to avoid the checkboard effects [53]. The linear filter presented by Pizzolato et al. [28] is implemented considering a filtering radius equal to $1.1 \bullet h_{el}$, while the smoothing of the design variable gradients caused by the filtering techniques is adjusted by the hyperbolic tangent projection operator equal to 0.5. The continuation scheme adopted for the projection parameter, the SIMP penalization exponent, and the TANH penalization coefficient are reported in Table 1 for a more exhaustive description of the filtering and regularization process, the interested reader is referred to [28]. The GCMMA was adopted as an optimization routine to update the material density after each optimization iteration, and the optimization process is terminated after 150 iterations [54]. The TO-based designs are reconstructed considering a cut-off parameter of *0.5* [55].Table 4.

4. Results and discussion

The multi-physics modelling approach adopted in this work (see governing equations in Section 3.2) allows to represent and predict the physical phenomena underpinning the performance of the TCS reactor. In this regard, typical global performance histories for the reactor design adopted for the model validation [33] are reported in Fig. 7. Here, the temperature and pressure histories, defined as the volume-averaged values across the reactive bed for a given design are reported. The histories of such average values are compared with the equilibrium and operating conditions. The equilibrium conditions refer to the volume averaged temperature and pressure values computed from equation (3.5), while the operating conditions refer to the volume-averaged temperature and pressure predicted during the discharge process.

Concerning Fig. 7 (a), the difference between the average TCM temperature, T_{TCM}, and the HTF temperature, T_{HTF}, indicates the temperature driver for the heat transfer from the porous bed to the heat transfer fluid. Such temperature driver varies depending on the HCM architecture, as more efficient extended surface geometries can boost the bed cooling and ultimately reduce the bed temperature. On the other hand, the difference between the bed temperature and the equilibrium temperature, T_{eq}, is proportional to the disequilibrium driver for the reaction kinetics (equation (3.4); the larger this difference, the larger the reaction rate, $\dot{\alpha}(\mathbf{s})$. Consequently, efficient cooling of the reactive bed also benefits the reaction rate.

Concerning instead the pressure histories, Fig. 7 (b), the disequilibrium driving the reaction rate is proportional to the difference between the average vapour pressure in the bed, p_v, and the equilibrium pressure, p_{eq}, with the latter derived from the solution of equation (3.5) for the volume average bed temperature, T_{TCM}. The pressure driver for the vapour transfer in the reactive bed is proportional instead to the difference between the average water vapour in the reactive bed and the vacuum chamber conditions. A low-pressure difference is desired, which indicates good mass transfer efficiency for the reactive bed. The prediction for the investigated TCS reactor exhibits a difference <100 Pa.

Table 4
Continuation scheme for the projection parameter, β, for the SIMP penalization exponent, p_{SIMP}, and for the TANH scheme penalization coefficient, p_{TANH}.

	1-30	31-60	61-90	91-120	121-150
β	1.0	2.0	2.0	4.0	8.0
p_{SIMP}	1.0	2.0	4.0	6.0	10.0
p_{TANH}	1.0	2.0	3.0	6.0	10.0

Literature studies indicate such difference to be influenced by the material properties and TCS geometry [6,31], nonetheless, it was predicted to be negligible compared to the imposed inlet vapour pressure value of $p_{v,\ in}$ (67 kPa) for all the design cases explored in this work. That is, a negligible influence of the vapour pressure distribution on the local and global performance of the investigated medium-temperature TCS reactor employing monohydrate strontium bromide was predicted, in agreement with the experimental and numerical conclusions reported in [5,33].

4.1. Optimal designs

In this section, the proposed optimization approach is adopted to generate optimal reactor designs and to assess the performance benefits achieved compared to literature benchmarks. A desired discharge time, t^*, of 1 h is selected for the analysis. Fig. 8 shows the design evolution along with the optimization iterations in the instance of the EOM problem. As discussed in Section 3.1.1, in the Energy Output Maximization (EOM) problem the packing factor is not prescribed, but rather an output of the optimization. Nonetheless, an upper boundary for the optimal packing factor of V*=0.4 was imposed to avoid the generation of impractical final designs. The initial design depicted in Fig. 8 corresponds to an initial homogeneous material distribution equal to the selected V^*. In agreement with the selected colour bar, the white areas refer to the TCM regions, while the black areas refer to the HCM regions. Thus, given the limited interpolation penalization imposed in the initial steps of the continuation scheme, a limited amount of enhancer material is ultimately distributed in the ground domain, with the packing factor value of ≈0.05. At iteration 30, the adopted continuation scheme dictates a variation in the optimization parameters, which leads to a sharp increase in both the objective function and packing factor values. Thus, more crisp design features emerge at iteration 60, where the main and secondary branches can already be distinguished. The remaining optimization history does not present any significant design change, with the packing factor value reaching the final optimal value of 0.18. The final design, i.e. iteration 150, presents a clear material transition contour, with limited use of grey material.

In a similar fashion, a MUM design was generated for a constraint $V^* = 0.1$. As discussed in Section 3.1.1, in the Material Utilization Maximization (MUM) problem the prescribed V* constraints the final design to a fixed packing factor, i.e. the amount of adopted HCM is heuristically selected prior to the optimization. The performance of both MUM and EOM designs was evaluated considering the interfacial thermal resistance and compared against a benchmark design. The benchmark design consists of a solution where 6 straight fins were evenly distributed across the reactive bed. It is worth noticing that such benchmark design has been widely investigated and adopted [11,20,56] as well as it has been demonstrated to be a suitable design for a range of different TCS materials [21,22,57]. Therefore, the selection of such relevant design benchmark i) allows to emphasize different design features the outcomes of topology optimization suggest to pursue in comparison with what is most commonly adopted so far, and hence ii) contributes to maximize the impact of our work by potentially informing and influencing a wider range researchers, academics and practitioners who are already familiar with the selected benchmark. The thickness of each fin was selected here to ensure the desired 0.1 packing factor, thus in agreement with the constraint set for the MUM optimization problem.

Fig. 9 shows the three designs considered. The MUM design presents 20 thin fins elongating from the HTF walls towards the vacuum chamber. No bifurcations are present, although a change in the fins' orientation is observed. Bifurcations are instead present in the EOM design. Here, thicker fins are found as no constraint on the packing factor is imposed in the optimization problem. Such thicker fins allow for more effective heat transport in the regions away from the HTF wall, and thus for a larger utilization of the material stored in such regions. Besides, the length of the first fin branch, i.e. the one in contact with the central pipe,

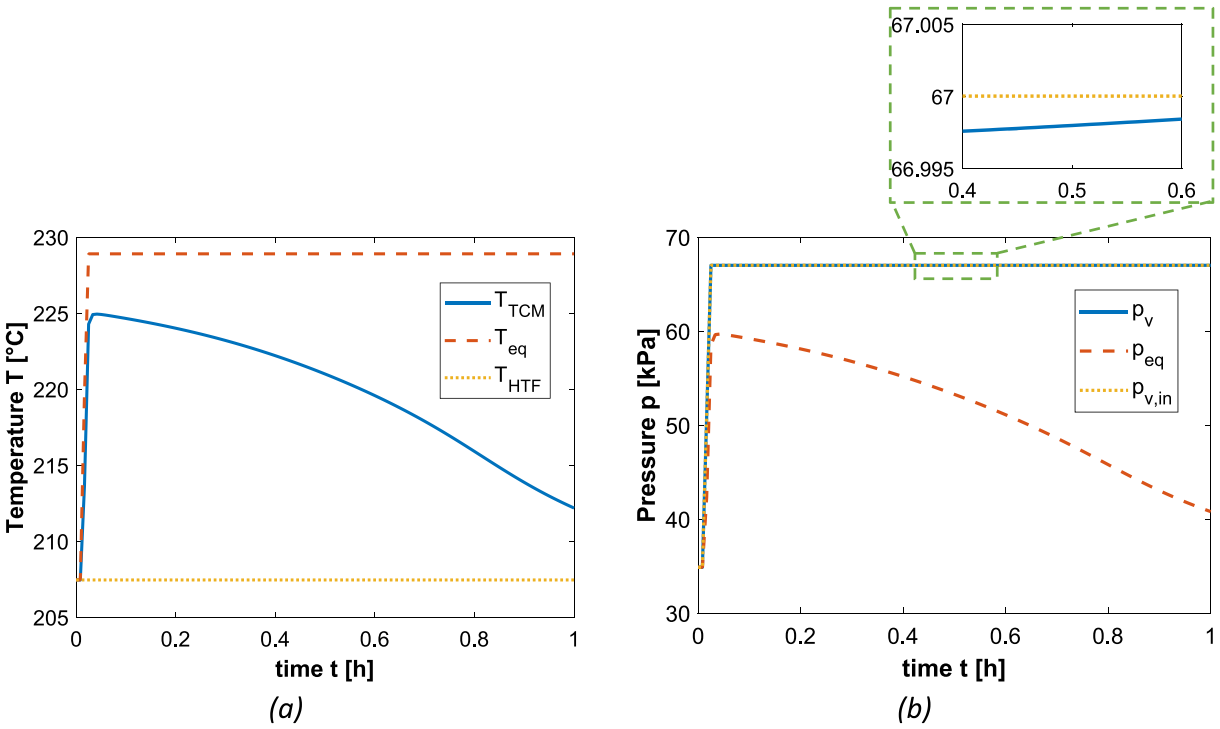

Fig. 7. Typical global histories for: (a) average temperatures; (b) average vapour pressures.

is not necessarily the same for all the branches. Rather, in the specific design of Fig. 9 (a), there is a succession of long-short-long first branches along the circumferential direction. These distinct characteristics are a direct result of the implemented Topology Optimization (TO) approach and hold significant implications for the optimal design within the specific case under examination. This is an exemplification of how, TO optimization, provides enhanced design freedom and thus design tunability with respect to traditional approaches, e.g. [14], where the length of each branch at a given bifurcation level is a priori assumed by the investigator to be identical for each fins.

The global performance histories are depicted in Fig. 10 for each of the three designs in Fig. 9. Concerning the reaction advancement, larger material utilization is achieved by the EOM design. This might seem counter-intuitive, as the maximization of the reaction advancement was adopted as the objective function for the MUM problem. The achievement of a larger α_{t^*} is dictated by the larger final packing factor, 0.18, compared to the one imposed volume in the MUM problem. The use of a larger packing factor implies in fact a lower storage material content in the reactive bed. Nevertheless, the MUM design, which ultimately entails similar storage material volume compared to the benchmark design, is predicted to lead to a final reaction advancement increase, $\Delta\alpha_{t^*}$, up to +0.27.

The amount of discharged energy is instead compared on the basis of the bed volume, which is calculated by accounting for both the volume devoted to the storage material and the volume devoted to the HCM. In Fig. 10 (b), a larger amount of energy is discharged from the EOM design, highlighting the importance of the proper packing factor selection to maximize the amount of energy retrieved from a fixed volume of space. A nearly threefold E_{t^*} is predicted for the EOM design compared to the benchmark design (+286%). Furthermore, a +44% increase is also estimated compared to the MUM design, concluding that the proposed TO framework allows generating designs with superior effective energy storage density at the reactor scale compared to conventional TES devices optimization.

The performance enhancement identified using the TO algorithm can be further appreciated in the reaction advancement contours depicted in Fig. 11. Here, a sharp reaction front is predicted to advance from the HCM and HTF walls, clearly showing that heat transfer is the main phenomenon limiting the hydration reaction. A closer look at Fig. 11 reveals that, although vapour transport occurs from the outer region toward the central pipe, the reaction advancement is instead initiated at cooled surfaces, namely the pipe and the fins. Although it might appear counterintuitive at first look, such behaviour is characteristic of TCS reactors whose physical behaviour is heat-transfer dominated. Indeed, results are in agreement with [31,33,44] which also demonstrate that reactions initiate near cooled surfaces and in areas where a local strong heat transfer occurs.

Poor reaction advancement is instead predicted for the benchmark design; such limited performance is caused by the large distance, on average, between the extended surface walls and the reaction sites. On the other hand, almost no unreacted TCM regions are observed in the EOM design. Given the imposed packing factor, the MUM design maximizes the reaction advancement primarily in the regions near the HTF wall, while a fraction of unutilized storage material is predicted in the regions near the vacuum chamber boundary.

The evolution of temperature contours over time for the EOM, MUM, and benchmark designs is presented in Fig. 12. For the EOM design, there is a noticeable trend towards temperature homogenization as time progresses. This implies that differences between the colder and warmer regions become less pronounced with increased discharge times. The most effective cooling effects are observed in the inner parts of fins bifurcations, dictated by the proximity to the HCM interfaces. In contrast, the MUM design demonstrates a cooling effect predominantly in the inner regions, i.e. close to the HTF pipe, of the reactive bed. Warm areas are mainly situated near the vacuum chamber. This characteristic can be attributed to the packing factor constraint applied during optimization. It results in optimal designs that mainly discharge the inner parts of the reactive bed within the chosen desired discharge time. The benchmark design, on the other hand, consistently exhibits higher temperatures. The temperature disparities between the warmest and coolest areas are subtle, with these variations exhibiting minimal shifts over time.

To further underscore the advantages of using TO as a design tool for TCS reactors, a MUM design was generated, maintaining the same conditions, dimensions, and packing factor (17%) as the experimental

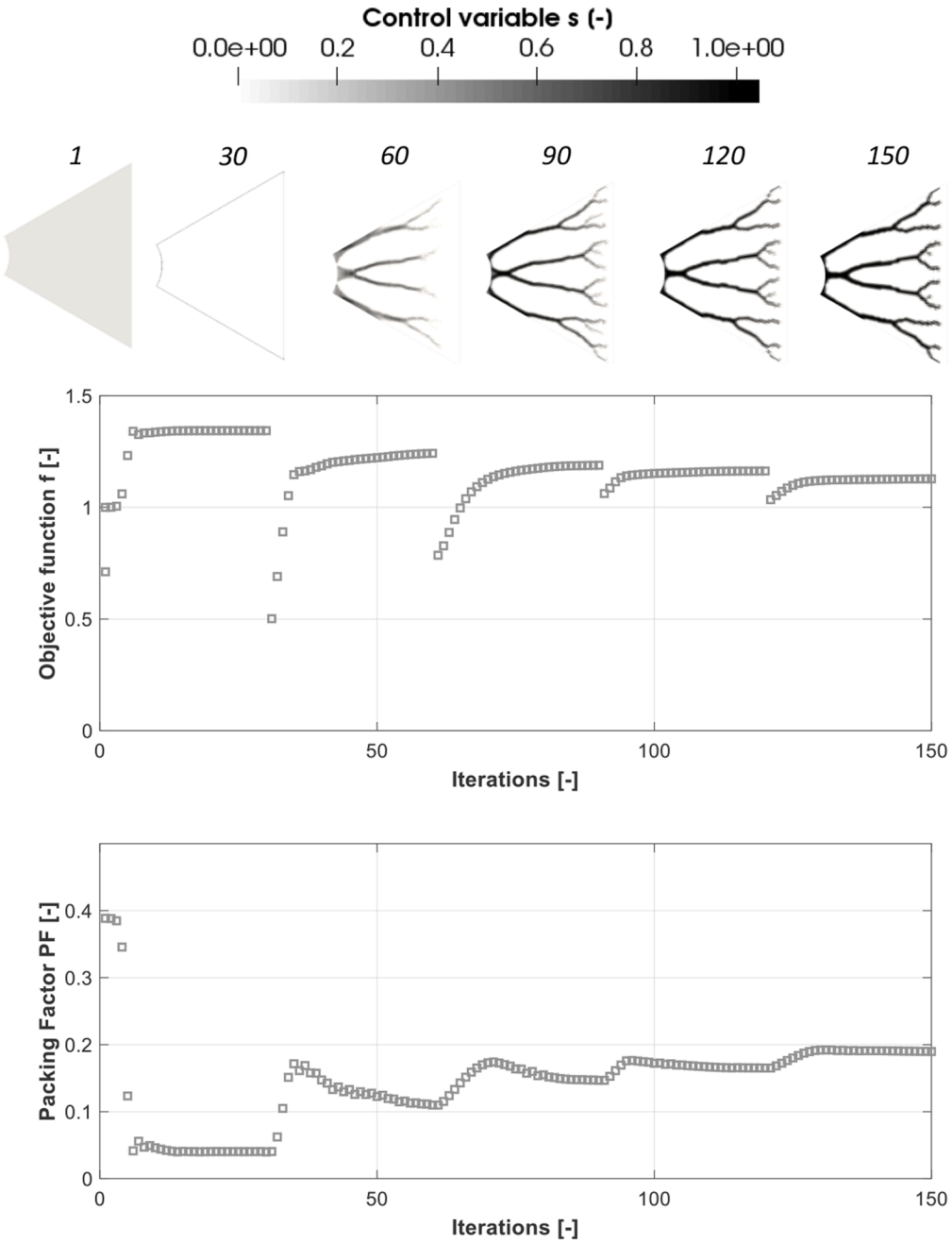

Fig. 8. Objective function and packing factor histories versus optimization iterations and design evolution before each continuation scheme step.

study by Stengler et al. [5]. In Section 3.2.3, it's detailed that the fin architecture tested in that study was heuristically developed to achieve high power density. However, the TO-generated design was forecasted to surpass the reference design, resulting in a 0.04 enhancement in final reaction advancement. This superior performance is attributed to the incorporation of a greater number of primary fins and the adoption of thinner fin profiles.

4.2. *Influence of the discharge time on the optimal design*

Through the application of the TO methodology, the optimal design emerges congruently with the designated objective function and the specific boundary conditions imposed. That is, the resultant optimal design is tailored to the unique design case considered, automatically generated by the TO algorithm, and lacking any preconceived assumptions. In this section, a systematic generation of optimal designs is undertaken to comprehensively investigate how varying discharge times, denoted as t*, impact the optimal design of HCM structures.

The optimal designs are compared in Fig. 13, considering both the MUM and EOM optimization problems and increasing t^* values. The majority of the optimal designs show main branches elongating along the diagonal of the hexagonal cross-section. This is an interesting result from the optimization algorithm: for design cases characterized by the variable distance between the HTF interface and the adiabatic boundaries, HCM branches need to be placed where the distance is maximum. Additional main branches emerge in the central part of the ground domain. The number of fins differs depending on the adopted optimization problem.

Regarding the MUM designs, the fins tend to stretch further across the ground domain for increasing t^* values. In other words, denser HCM distributions near the HTF wall are suitable in case of shorter discharging times, as the energy can be mainly retrieved from these

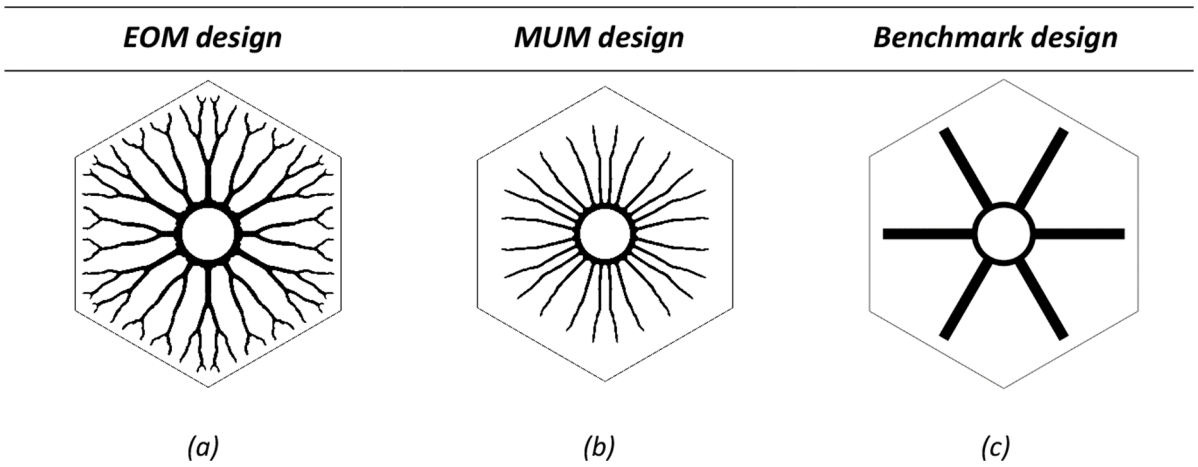

Fig. 9. Comparison of the optimization design and benchmark design: (a) EOM design; (b) MUM design; (c) benchmark design with straight fins.

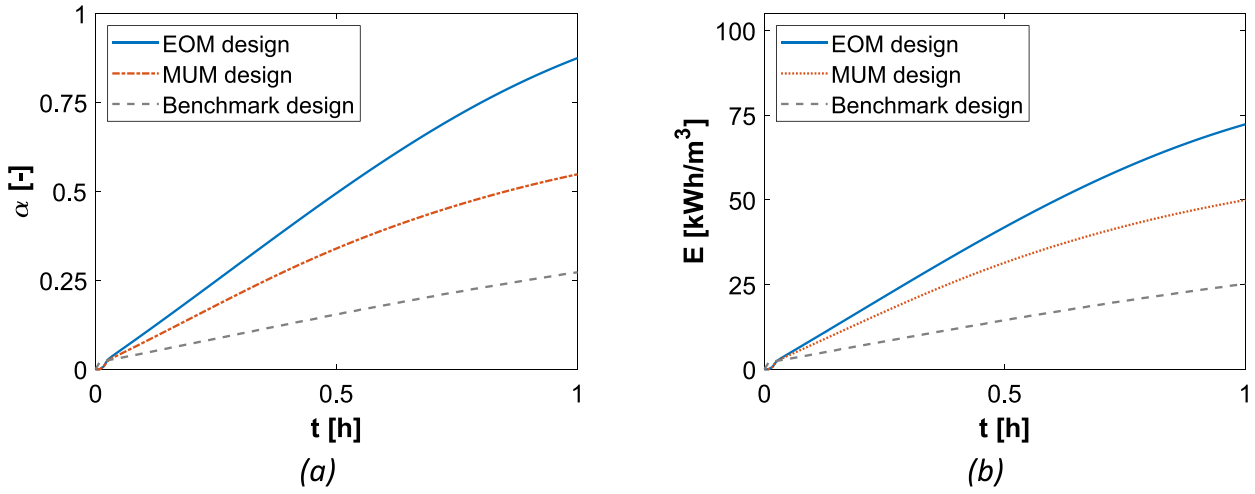

Fig. 10. Comparison of the reaction advancement and discharged energy histories for the optimal designs and literature benchmarks.

regions. Nevertheless, relatively poor material utilization is achieved in the instance of short discharge times. When the EOM problem is considered, a different trend is observed. Here, a large fraction of the ground domain is dedicated to the enhancer material, up to 38%, in the case of short discharging times. The emerging optimal design is complex, characterized by several fin bifurcations and wavy profiles. Besides, isolated TCM regions emerge in the final design for time $t^* = 0.2\ h$. In fact, despite the mass transfer penalization strategy described in section 3.3.2, vapour is still predicted to be transferred in these regions in the TO framework. As a consequence, the TCM contained in the isolated regions is predicted to contribute to the enhancement of the amount of energy discharged from the ground domain.

However, the TCM located in isolated regions cannot be exploited in a real TCS system, as no vapour can be provided. As a result, the energy density of the reconstructed design was penalized. For increasing t* values, a lower optimal packing factor was derived from the EOM problem (down to 0.18). Finally, in the instance of $t^* = 2.0\ h$, the HCM is mainly distributed in the proximity of the vacuum chamber interface in order to favour the heat transfer away from the HTF interface.

As can be appreciated in Fig. 13, the designs generated from the TO algorithm are characterized by complex geometrical features, which might raise questions regarding their manufacturability. While the realization of the optimal designs is out of the scope of this work, considerations regarding possible fabrication routes are presented in section 5.

The objective function values versus the desired discharge time are depicted in Fig. 14, considering both the TO framework results and the re-evaluated performance accounting for the interfacial thermal resistance. Again, higher final reaction advancements are predicted for the EOM designs due to the larger packing factor, i.e. lower TCM content in the ground domain. The largest performance discrepancy is observed in the instance of $t^* = 1$ h, with the EOM design predicted to deliver +47% energy compared to the MUM design, as already discussed in the previous section.

However, when large desired discharge times are considered, e.g. $t^* = 2$ h, higher discharged energy is achieved here by means of the MUM design for the TO framework. The authors believe this result to be caused by the large reaction advancement achieved in the physical model, $\alpha_{t^*} \approx 1.0$, which ultimately makes local minimum appear in the optimizer routine. Nevertheless, in the instances of $\alpha_{t^*} < 0.96$, the objective function values reported in Fig. 14 highlight that the design generated by TO remains nondominated solutions also when the interfacial effects are considered. That is, the overall methodology presented in this work is reliable for the generation of fit-for-purpose designs. For a clearer representation of the results, the design performance presented hereafter solely refers to the numerical predictions where the effect of h_{int} is considered.

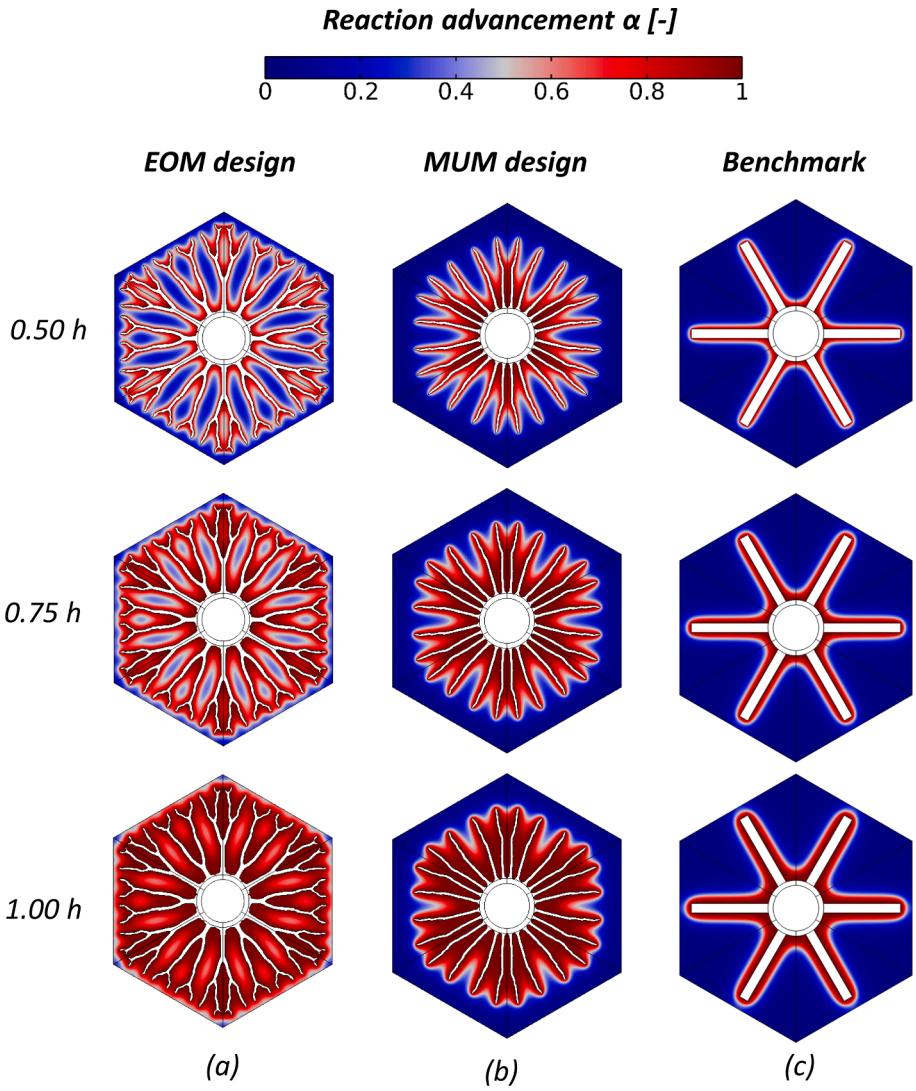

Fig. 11. Reaction advancement contours evolution in time for: (a) Energy output (EOM) design; (b) Material Utilization Maximization (MUM) design (c) benchmark design. EOM and MUM are defined in Section 3.3.1.

4.3. Effect of the bed size on the optimal design

In this section, the design trends for the optimal HCM distribution are analyzed for TCS reactors characterized by different bed sizes. Specifically, compared to the design cases presented in the previous sections, a reactive bed length *W* of *75 mm* and *100 mm* were considered as extensively detailed in Section 3.2.1. The analysis was carried out considering a fixed discharging time of *2 h* and operating conditions as per section 4.2. Fig. 15 shows the optimized designs. Concerning the MUM problem, the optimal number of branches varies depending on the value of *W*. In particular, instead of four main branches elongating from the HTF interface, the optimal design for *100 mm* and *75 mm* presents only two main branches with primary and secondary bifurcations.

Interestingly, the MUM design does not present main branches elongating along the ground domain diagonal, but rather two consecutive fins with a relatively small pitch. As a consequence, a small fraction of TCM is present along the ground domain diagonal. Such TCM region was predicted to hydrate in relatively short times, with the TCM hydration boosted by the large heat transfer enhancement effect provided by the fins. Furthermore, given the longer distance between fins and TCM material in the case of *100 mm* bed size, optimal designs with thicker fins were obtained, with a maximum thickness increasing from *1.1 mm* to *3.1 mm*, respectively, for the *50 mm* and *100 mm* designs. As a consequence, the HCM is not distributed in the regions away from the HTF interface, i.e. near the vacuum chamber, in case of larger bed sizes, with the fins elongating for a maximum distance from the HTF pipe centre of *0.76*W* versus *0.95*W*.

Concerning the EOM designs, more complex HCM architectures can be observed compared to the MUM designs. The fins present at least primary and secondary bifurcations, while the optimal packing factor increases with the reactive bed size. Indeed, a final packing factor of 0.18 was adopted in the case of medium size reactive bed, *50 mm*, while such a fraction increases to 0.3 for bed size of *100 mm*. Isolated TCM regions emerged in the instance of the EOM problem for *75 mm*. Again, while these regions are predicted to react, they lead to an unused fraction of storage material in the reconstructed design. To overcome this limitation, the portion of HCM depicted in red in Fig. 15 was manually removed in the reconstructed design.

Fig. 16 exhibits the predicted performance metrics versus the bed size. Large final reaction advancements ($> 80\%$) are achieved by designs found through the EOM problem regardless of the bed size, while a significant α_{t^*} reduction is observed in the instance of the MUM problem for increasing values of *W*. That is, for relatively large bed sizes, a 10% packing factor is not sufficient to obtain large material utilization factors. Similarly, the amount of energy discharged from the reactive bed is observed to reduce with the bed size, although relatively E_{t^*} value

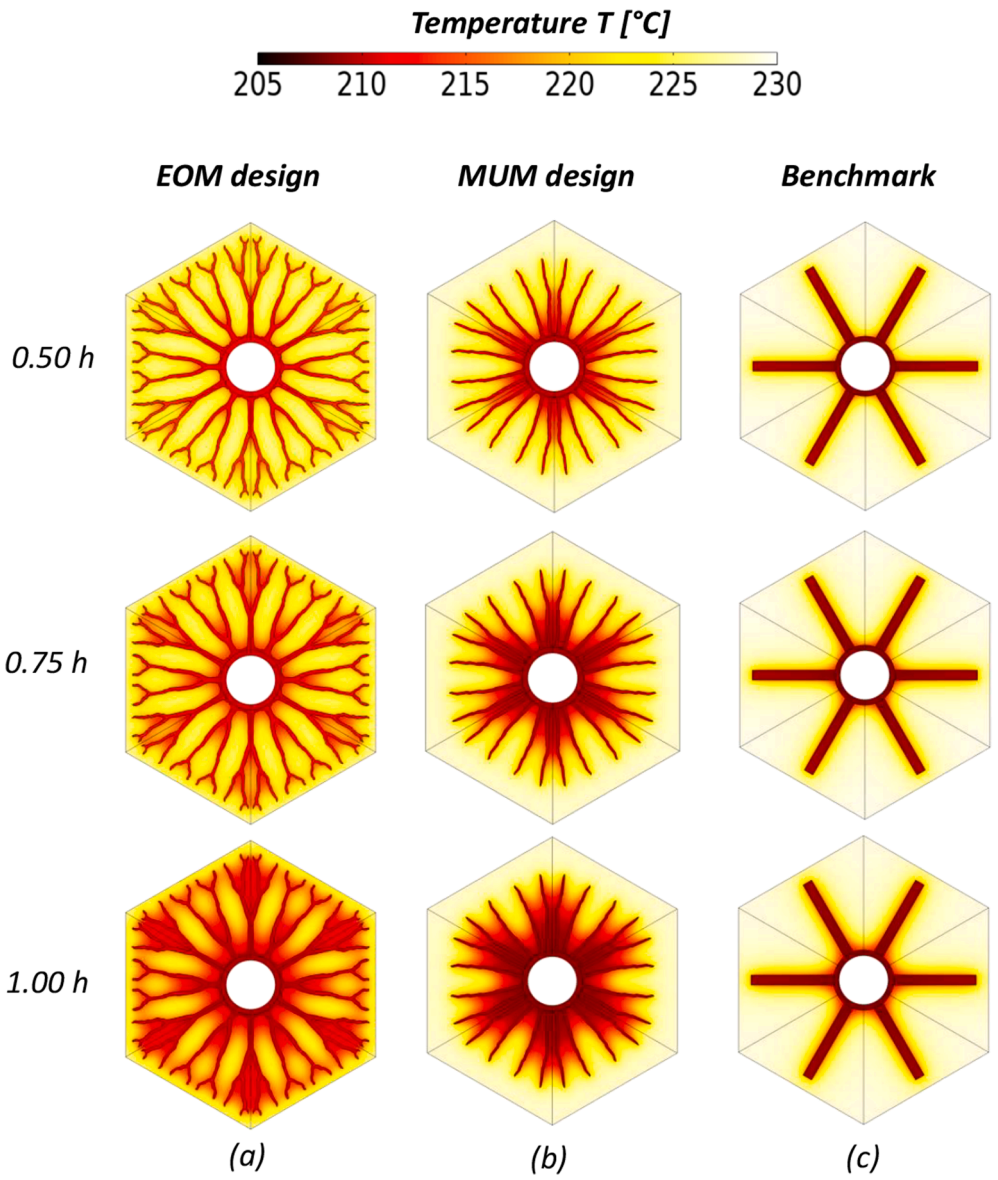

Fig. 12. Temperature contours evolution in time for: (a) Energy output (EOM) design; (b) Material Utilization Maximization (MUM) design (c) benchmark design. EOM and MUM are defined in Section 3.3.1.

reductions were predicted for EOM designs. As an additional performance indicator, the TCS reactor energy storage density was also evaluated. The TCS reactor energy storage density is defined as the amount of energy discharged from the reactive bed over the reactor volume and can thus be calculated as:

$$E_{t^*,r} = E_{t^*} \frac{V_{bed}}{V_{reactor}} \tag{4.1}$$

where $V_{reactor}$ is the reactor volume, calculated as the sum of the bed volume, the volume devoted to the HTF pipes and the volume devoted to the vapour diffuser channels, for which a 6 mm size is assumed [6,40]. The size of the HTF pipes and of the vapour diffuser channels are assumed constant with the bed size, W. That is, larger bed over reactor volume ratios are obtained for increasing W values. Interestingly, the predicted TCS reactor energy storage density, Fig. 16 (c), shows maximum values in the instance of the EOM problem at relatively high W values and a packing factor of 0.21. That is, the most performing reactor configuration is obtained for relatively large packing factor and a large distance between the HTF pipes.

Table 5 reports the optimal packing factor values resulting from the EOM problem. The optimal packing factor does not linearly scale with the bed size. In fact, a relatively small increase is observed between the 50 mm and 75 mm cases, ultimately contributing to the overall larger reactor energy storage density obtained for the latter case. On the other hand, a more significant increase is instead observed for W=100 mm, denoting the need for a large amount of enhancer material when a large distance between HTF pipes is selected.

4.4. Effect of the bed porosity on the optimal design

The influence of the bed properties on the optimal HCM architecture is explored in this section by varying the reactive bed porosity value, ε. The influence of the bed permeability, K, is instead disregarded in the analysis. In fact, as observed by Stengler et al. [33], given the high pressure adopted for the discharge process of medium-temperature TCS reactors, mass transfer in the reactive bed does not influence the reactor performance. The bed porosity was varied in the range of 0.30 to 0.69.

Fig. 17 presents the optimal HCM architecture for increasing bed porosity values. Concerning the MUM problem, the optimal fins tend to

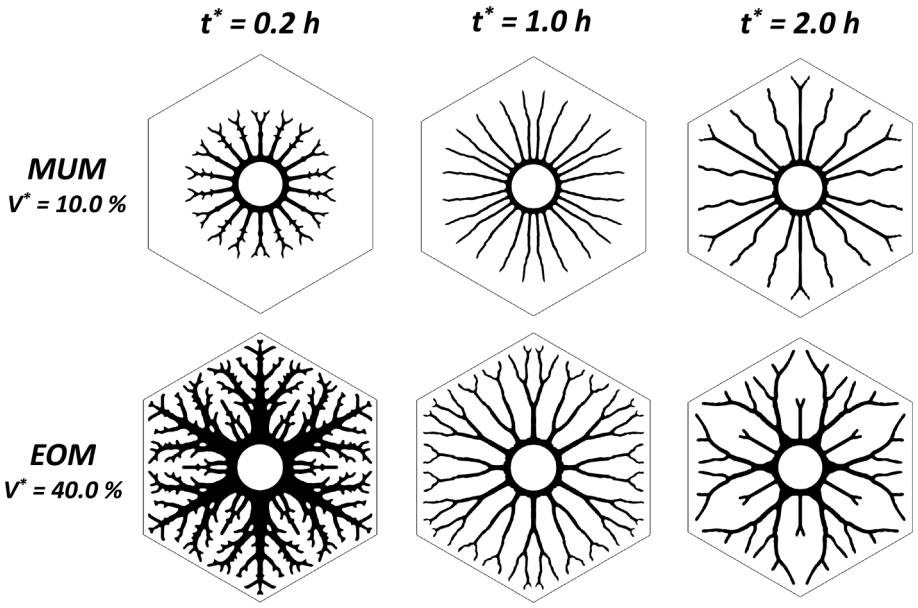

Fig. 13. Optimal designs for the material utilization maximization, MUM, and the energy output maximization, EOM, problems for increasing values of the desired discharging time, t*.

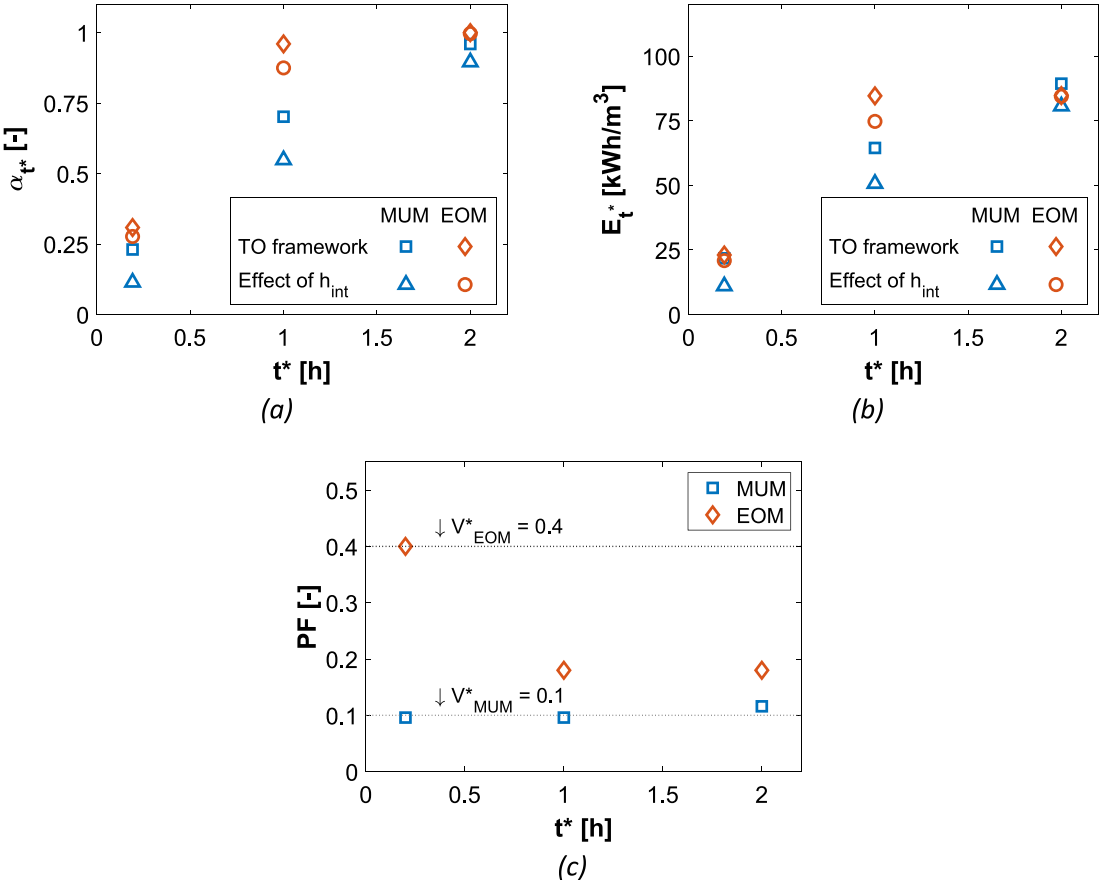

Fig. 14. Performance metrics comparison for the optimized designs: (a) final reaction advancement, α_{t^*}; (b) Discharged energy, $\mathbf{E}_{t^*}$; (c) Packing factor for the reconstructed designs, PF.

stretch towards the outer boundary in case of higher bed porosity, while a denser HCM distribution in the proximity of the HTF wall was found in the case of highly-packed TCM. Besides, thinner fins are obtained in the instance of large porosity. Both these trends are due to the energy content variation in the ground domain dictated by the porosity variation. In fact, reduced porosity values imply higher maximum energy densities, and thus a larger amount of energy potentially discharged in the desired time t^*. On the other hand, a more packed TCM also

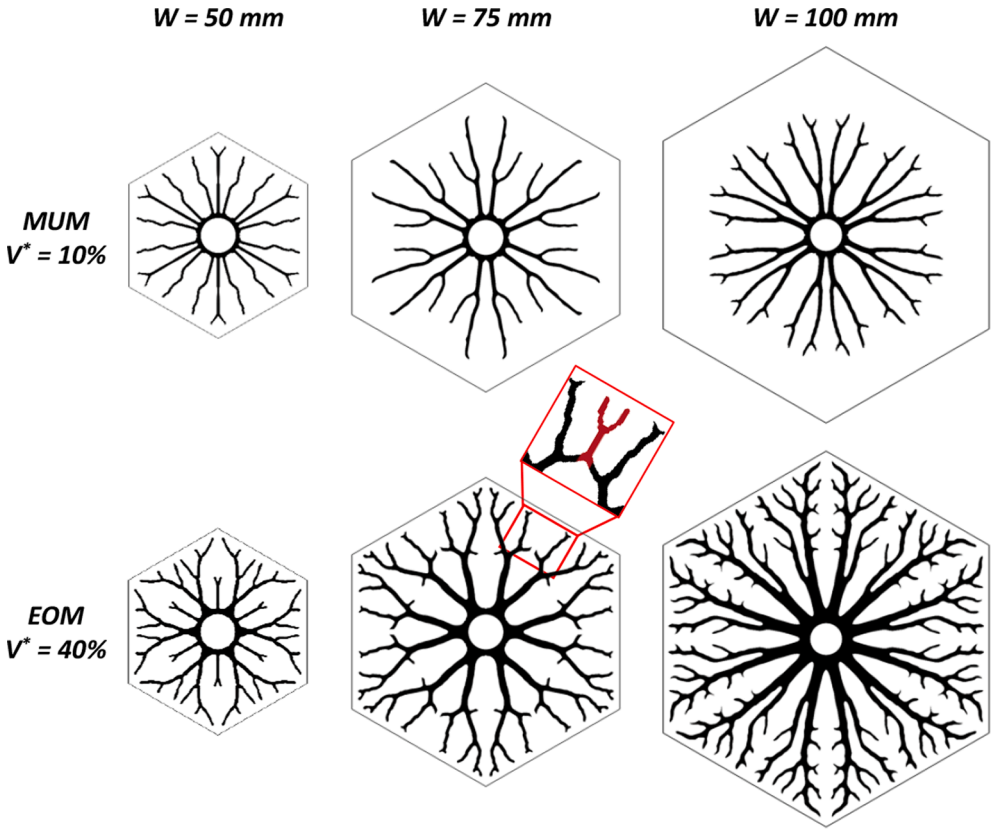

Fig. 15. Optimal HCM distribution derived from the material utilization maximization, MUM, and the energy output maximization, EOM, problems for increasing bed size, W.

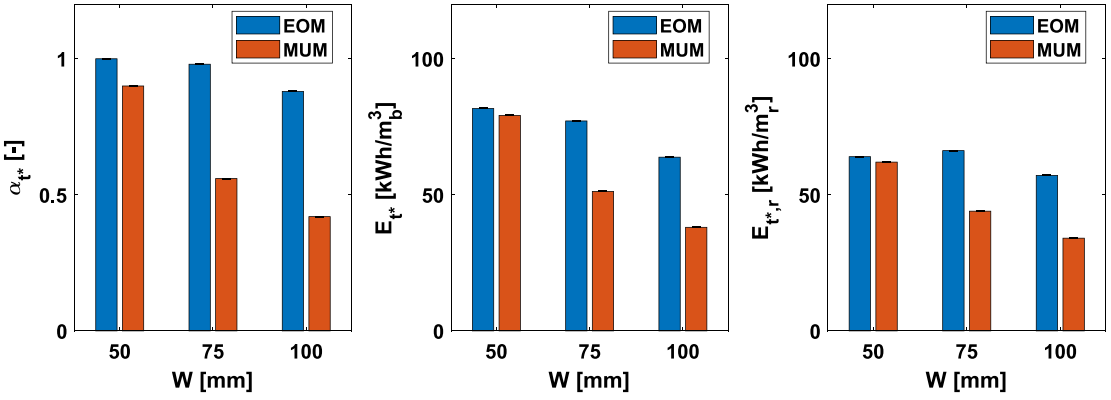

Fig. 16. Performance metrics comparison for the optimized designs at different bed sizes: (a) final reaction advancement, α_{t^*}; (b) discharge energy over bed volume, E_{t^*}; (c) discharged energy over reactor volume, $E_{t^*,r}$.

Table 5
Packing factor values for the optimal designs from the EOM and MUM problems for different bed sizes.

	EOM			*MUM*		
W [mm]	50	75	100	50	75	100
PF [-]	0.18	0.21	0.28	0.12	0.1	0.1

guarantees higher effective thermal conductivity, as $\lambda_{TCM} > \lambda_{vapor}$. As a result, while a significantly higher energy can be discharged in the case of $\varepsilon = 0.30$ compared to $\varepsilon = 0.69$ (Fig. 18), mild variations are predicted in terms of reaction advancement, i.e. the fraction of stored energy discharged in the time t*.

Concerning the EOM designs, thicker fins are again obtained for highly packed reactors, with the fins' thickness reduced for increasing ε values. The number of main branches does not vary with the bed porosity, although a larger number of ramifications was obtained for Digitare l'equazione qui. $\varepsilon = 0.3$ compared to higher values. This is again due to the larger energy content in the bed when ε is low, which leads to a more ramified HCM architecture to effectively retrieve the stored energy.

The EOM designs outperform the MUM designs regardless of the performance metric adopted, as shown in Fig. 18. Again, concerning α_{t^*}, this is dictated by the larger final packing factor PF value. Opposite trends in the two performance metrics are observed for increasing value of bed porosity. While the final reaction advancement increases with the bed porosity, the reactive bed energy storage density decreases. That is,

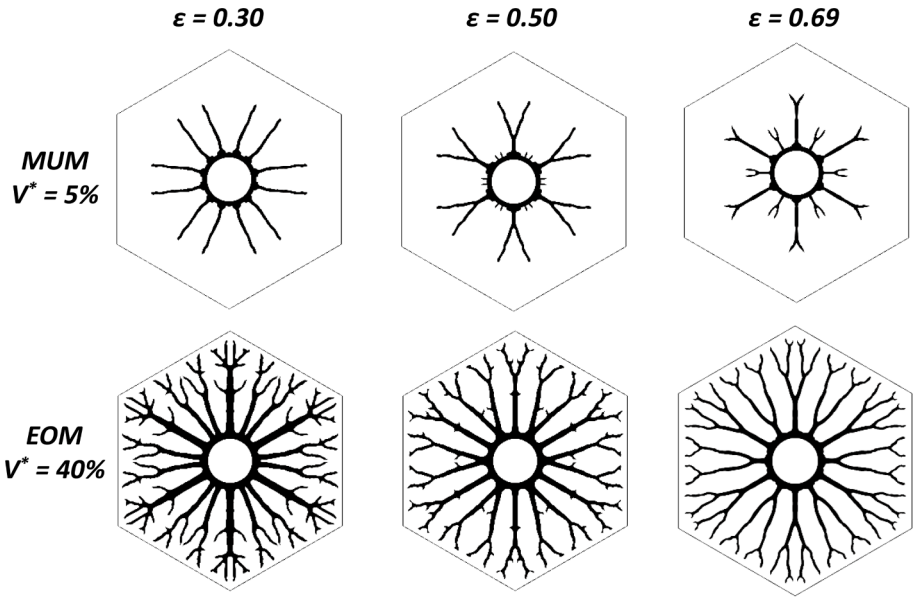

Fig. 17. Optimal designs for the material utilization maximization, MUM, and the energy output maximization, EOM, problems for increasing values of the bed porosity, ε.

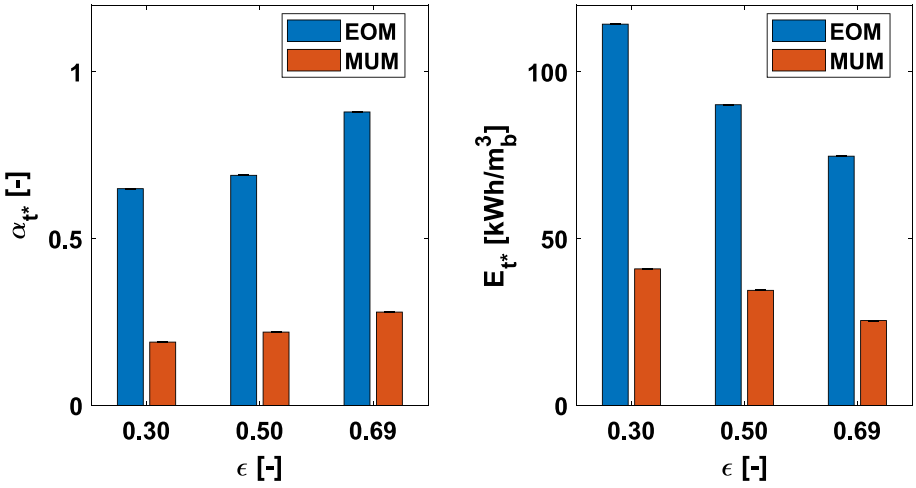

Fig. 18. Performance metrics comparison for the optimized designs for different porosity values: (a) final reaction advancement, α_{t^*}; (b) discharge energy over bed volume, E_{t^*}.

larger material utilization is achieved by choosing a less packed reactive bed, leading, therefore, to a larger retrieved energy per mass of storage material. On the other hand, a more packed reactive bed increases the amount of energy discharged in the selected desired discharge time. In fact, the selection of highly packed bed reactors, $\varepsilon = 0.3$, leads to a discharged energy increase up to +57.0 kWh/m^3 compared to beds presenting high void fractions, $\varepsilon = 0.7$. Such a larger bed energy storage density is obtained despite an increase in optimal packing factor (+0.09), as shown in Table 6. Again, this is an interesting result, demonstrating how maximized performance can be obtained by highly packed reactors adopting relatively large packing factor values.

Table 6
Packing factor values for the optimal designs from the EOM and MUM problems for different bed porosity values.

	EOM			*MUM*		
ε [-]	0.30	0.50	0.69	0.30	0.50	0.69
PF [-]	0.27	0.21	0.18	0.05	0.05	0.05

4.5. Considerations on manufacturing of optimal designs

This section provides recommendations regarding the fabrication of the optimal designs. The non-intuitive geometrical features that emerged from the topology optimization algorithm were demonstrated in this work to provide significant performance enhancement; however, these geometrical features might raise questions regarding the manufacturability of the optimal design.

In these regards, two possible routes for the fabrication of the TO designs are envisioned:

(i) Direct fabrication via additive manufacturing;
(ii) Fabrication of TO-inspired designs with conventional manufacturing techniques;

In contrast with conventional manufacturing methods, additive manufacturing offers increased flexibility which enables the fabrication of complex geometrical features made of copper, aluminium, ferrous materials, etc. [58]. Additive manufacturing is, thus, an enabling

technology that allows designers to overcome the current manufacturing limitation that inhibits the adoption of topology optimization. In recent years, additive manufacturing of topologically optimized thermal devices has been growing rapidly [59], as several successful examples have been reported in the literature. For example, Lazarov et al. [60] manufactured and tested TO-based designs for LED light cooling, for which a 50% decrease in operational cost was measured compared to conventional designs. Furthermore, in one of our previous works, we demonstrated the use of selective laser melting additive manufacturing as a manufacturing route for directly fabricating a TO-based design of a multi-tube shell-and-tube latent heat thermal energy storage device [61]. Stengler et al. [5] tested complex branched fins geometries in the context of closed system TCS reactors, thus in close proximity with the study presented in this work. The operation of a small-scale (1 kW) reactor was demonstrated in a vast range of operating conditions (1 to 560 kPa). Nonetheless, the design considered for the study was adapted from a different thermal device [62] and thus was not specifically designed to maximize the behaviour of the TCS reactor.

However, while additive manufacturing cost is foreseen to reduce in time [63], this route is still not a cost-effective solution in most cases. Fabrication route (ii) entails using the TO results as design guidelines for generating highly manufacturable final designs. The TO designs can be interpreted by the designers and recreated by adopting highly manufacturable geometrical features. For example, Pizzolato et al. [19] presented the skeletonization of optimized fins in a latent heat energy storage device. A discharge time increase of 5% was predicted for the highly manufacturable design compared to the topological design. While these post-processing steps were performed manually in Pizzolato's work, numerical strategies have already been presented in the literature for systematic design post-processing to ensure manufacturability [64,65].

To limit the manufacturing cost, we envision manufacturing route (ii) as the preferred one. Nonetheless, it is crucial to stress that the proposed optimization approach is necessary to systematically identify the key geometrical features that greatly benefit performance. At the same time, post-processing techniques can be adopted to ensure the feasibility of these geometrical features and to ultimately manufacture high-performing reactors.

5. Considerations on limitations and potential for future work on topological optimization of TCS systems

This study focused on TO of a reference TCS reactor originally conceived to target heat storage in potential industrial applications requiring reactor concepts explicitly designed for high specific thermal power. Results clearly demonstrate that TO allows to develop designs with performance remarkably higher that the state-of-the-art TCS reactor design. We therefore believe the present study has the potential to be an initial platform upon which further TO research could be based upon. In this regard, this section highlights potential areas for further research work.

As extensively detailed in Section 3 the proposed TO modelling framework was developed considering assumptions that have been successfully adopted in recent state-of-the-art works in literature. Nonetheless, we would like to point out a number of such assumptions and the related potential for future work that could be carried out beyond the scope of the present work:

- *Application scenarios*: This study focused on TO of a reference TCS reactor conceived for heat storage in potential industrial applications. Nonetheless, the applications of TCS are rapidly expanding [66]; thus, future TO research work could be directed at addressing the development of TCS reactors for applications scenarios different from the one addressed in the present work. Of particular interest is TO of compact TCS reactors for long duration thermal energy storage in buildings.
- *Operating conditions*: This study considered specific operating conditions (vapour pressure and temperature) and discharge times. Clear trends in the TO designs have been identified for such conditions. Still, future work could be done to fully examine the effect of different operating conditions and operating strategies on the optimality of the designs, and how robust these optimal designs are. This work exclusively focused on the discharge process of a TCS reactor, as this regulates the amount and quality of the heat delivered to the users. However, existing literature has highlighted conditions where the charging process could potentially impede the effective functioning of a TCS system [67]. Furthermore, previous research in the field of latent heat thermal energy storage showed TO-designs to differ when full charge/discharge cycles are considered compared to the ones emerging from the study of the single processes [68]. More broadly, we do see the need for robust optimization of TCS systems regardless of the optimization technique adopted since the majority of design optimization studies do not fully account for variability and uncertainty in operating conditions.
- *TCS Reactor dimensions and TCS materials*: This study identified how the TO designs varied in relation to a specific range of TCS reactor dimensions. As outlined in Section 3, the dimensions selected for TCS reactors might vary significantly depending on the intended application and the associated performance target. We, therefore, recommend setting up TO for the range of dimensions of the TCS reactor dimension expected for the intended application scenario (point 1 above). Nonetheless, tradeoff between the number of designs for different TCS reactor dimensions and computational costs should be pursued. This is essential not only to ensure efficient use of computational resources but also interpretability of design trends. Finally, exploring the relationship between the optimized geometry and TCS materials different from the one considered in another area where further TO work could be done.
- *3D designs*: This study identified TO designs following a two-dimensional modelling approach, which has been proven successful in the literature as discussed in Section 3.2. Nonetheless, the TO framework proposed in this work is directly applicable to a 3D analysis. Depending on the intended application, full 3D topological design might be relevant. For example, in the instance of large TCS reactor volumes, there could be non-negligible pressure difference along the TCS reactor length. Such non-uniform conditions, in turn, might in principle lead to optimal designs with features that vary along the length of the TCS reactor as well. i.e. a topology that varies long the length of the TCS reactor.

However, we do highly recommend to perform two-dimensional TO first. As shown in our previous work on other TES systems [28], 3D TO that accounts for variations along the TES system easily leads to geometries far more complex than the two-dimensional case and further significant performance improvement beyond those achieved by two-dimensional design is not given for granted. Further, how to formally include manufacturing constraints into the mathematical formulation of TO remains by and large an unanswered question in the TO research field. Hence, trade-offs between performance benefits, manufacturability, computational costs and results interpretability should be carefully considered prior to embarking on 3D design. Rather, as pointed out in Section 5, we recommend pursuing *TO-inspired designs*. That is, employ TO for exploring the design space and use the TO results as design guidelines to generate design options to be compared with current alternatives. A potentially promising approach to generating pseudo-3D designs consists of the extrusion of two-dimensional optimal designs [28].

Once the extent of the performance improvement achieved by *TO-inspired designs* is ascertained, the analyst could take an evidence-based decision on the cost-benefits of whether pursuing TO that includes further details (e.g. full 3D optimization). The results presented in this work clearly demonstrate that, in the context of the intended application

of the TCS reactor being studied and associated assumptions, a two-dimensional TO could already guide the analyst toward performance improvements in the order of ~ +200%.

6. Conclusions

In this work, the use of topology optimization for the effective design of thermochemical energy storage devices employing gas/solid reactions was demonstrated. The optimal geometries of extended surfaces were generated for multiple desired discharge times, bed sizes and bed properties. From the results presented in this work, the following conclusions can be derived:

- Under the considered assumptions, the optimization approach presented in this work can generate designs with superior performance compared to state-of-the-art solutions. For a fixed desired discharge time and fixed packing factor value, a final reaction advancement enhancement up to +0.27 is predicted;
- The application of a novel optimization problem formulation, referred to as the energy output maximization problem, allowed for the generation of optimal designs without the need for a prescribed packing factor, which is a further novelty of the study. For a fixed desired discharge time, the energy output maximization problem led to an increase of discharged energy up to +47.0% compared to a conventional approach adopted for the optimization of TCS devices;
- The emerging design trends show that the investigated design parameters largely influence the optimal extended surface architecture and the optimal packing factor value. The optimal packing factor value significantly reduces with an increase in discharge time and increases with the bed size. Nevertheless, the maximum reactor energy density is obtained through a relatively high packing factor value of 21% and a larger bed size. This solution was found to effectively mitigate the influence of dead volumes, i.e. volume devoted to the heat transfer fluid pipes and reactants distribution channels, on the overall reactor energy density;
- Thicker fins are favourable in low porosity beds, with the number of fins varying only when a relatively small packing factor constraint is imposed. The maximum amount of retrieved energy from the thermochemical energy storage reactor was predicted for highly packed bed reactors employing a relatively high packing factor value, with enhancements up to +57 kWh/m^3 compared to less packed beds utilizing optimized fins.

Overall, the results demonstrate that topology optimization constitutes a highly valuable and thorough design tool for the generation of fit-for-purpose designs. In this sense, three fundamental and overarching concluding remarks can be drawn: (i) the proposed topology optimization approach leads to designs with markedly higher performance than traditional configurations commonly proposed (ii) the topological optimization approach gives access to designs that are not attainable by traditional approaches or by means of heuristic methods iii) the inspection of the topologically optimized configuration, together with the corresponding optimization problem formulation, and the predicted results provide new understanding on the causal correlations between physical phenomena, geometry and performances. This latter point is particularly relevant and unique to the framework and approach demonstrated here. In other words, the topological engineering approach abates uncertainty, reduces heuristics and provides actual systematic insight into what could unlock performance in energy devices. Opportunities for further research and extension of the proposed TO framework have been also outlined and discussed. Therefore, the results presented in this work ultimately contribute to the generation of design guidelines and provide fundamental insights for advancing thermochemical energy storage technology as well as advancing topological optimization into a novel application field.

Declaration of competing interest

The authors declare that they have no known competing financial interests or personal relationships that could have appeared to influence the work reported in this paper.

Data availability

Data will be made available on request.

References

[1] D. Lefebvre, F.H. Tezel, A review of energy storage technologies with a focus on adsorption thermal energy storage processes for heating applications, Renew. Sustain. Energy Rev. 67 (2017), https://doi.org/10.1016/j.rser.2016.08.019.
[2] L.F. Cabeza, A. Solé, C. Barreneche, Review on sorption materials and technologies for heat pumps and thermal energy storage, Renew. Energy 110 (2017) 3–39, https://doi.org/10.1016/j.renene.2016.09.059.
[3] B. Michel, N. Mazet, P. Neveu, Experimental investigation of an innovative thermochemical process operating with a hydrate salt and moist air for thermal storage of solar energy: global performance, Appl. Energy 129 (2014) 177–186, https://doi.org/10.1016/j.apenergy.2014.04.073.
[4] D. Aydin, S.P. Casey, X. Chen, S. Riffat, Novel, "open-sorption pipe" reactor for solar thermal energy storage, Energy Convers Manag 121 (2016) 321–334, https://doi.org/10.1016/j.enconman.2016.05.045.
[5] J. Stengler, M. Linder, Thermal energy storage combined with a temperature boost: An underestimated feature of thermochemical systems, Appl. Energy 262 (2020), 114530, https://doi.org/10.1016/j.apenergy.2020.114530.
[6] G. Humbert, Y. Ding, A. Sciacovelli, Combined enhancement of thermal and chemical performance of closed thermochemical energy storage system by optimized tree-like heat exchanger structures, Appl. Energy 311 (2022), 118633, https://doi.org/10.1016/J.APENERGY.2022.118633.
[7] L. André, S. Abanades, Recent advances in thermochemical energy storage via solid–gas reversible reactions at high temperature, Energies 13 (2020), https://doi.org/10.3390/en13225859.
[8] L. Scapino, H.A. Zondag, J. Van Bael, J. Diriken, C.C.M. Rindt, Sorption heat storage for long-term low-temperature applications: A review on the advancements at material and prototype scale, Appl. Energy 190 (2017) 920–948, https://doi.org/10.1016/j.apenergy.2016.12.148.
[9] A.H. Abedin, M.A. Rosen, Closed and open thermochemical energy storage: Energy- and exergy-based comparisons, Energy 41 (2012) 83–92, https://doi.org/10.1016/j.energy.2011.06.034.
[10] P. Neveu, S. Tescari, D. Aussel, N. Mazet, Combined constructal and exergy optimization of thermochemical reactors for high temperature heat storage, Energy Convers Manage. 71 (2013) 186–198, https://doi.org/10.1016/j.enconman.2013.03.035.
[11] G. Papakokkinos, J. Castro, J. López, A. Oliva, A generalized computational model for the simulation of adsorption packed bed reactors – Parametric study of five reactor geometries for cooling applications, Appl. Energy 235 (2019) 409–427, https://doi.org/10.1016/j.apenergy.2018.10.081.
[12] Wang B, Wang Z, Ma Y, Liang Y. Heat Transfer Enhancement of Indirect Heat Transfer Reactors for Ca(OH)2/CaO Thermochemical Energy Storage System. Process 2021, Vol 9, Page 1136 2021;9:1136. 10.3390/PR9071136.
[13] K. Kant, A. Shukla, D.M.J. Smeulders, C.C.M. Rindt, Analysis and optimization of the closed-adsorption heat storage bed performance, J Energy Storage 32 (2020), 101896, https://doi.org/10.1016/j.est.2020.101896.
[14] K. Kant, R. Pitchumani, Analysis of a novel constructal fin tree embedded thermochemical energy storage for buildings applications, Energy Convers Manag 258 (2022), 115542, https://doi.org/10.1016/J.ENCONMAN.2022.115542.
[15] A. Malley-Ernewein, S. Lorente, Constructal design of thermochemical energy storage, Int. J. Heat Mass Transf. 130 (2019) 1299–1306, https://doi.org/10.1016/j.ijheatmasstransfer.2018.10.097.
[16] A. Malley-Ernewein, S. Lorente, Analysis of thermochemical energy storage in an elemental configuration, Sci. Rep. 9 (2019) 15875, https://doi.org/10.1038/s41598-019-52249-8.
[17] A. Malley-Ernewein, S. Lorente, Fishbone structures for thermochemical energy storage in porous systems, J Energy Storage 53 (2022), 105178, https://doi.org/10.1016/J.EST.2022.105178.
[18] G. Humbert, A. Sciacovelli, Topology optimization for mass transfer enhancement in open thermochemical energy storage reactors, J Energy Storage 64 (2023), 107132, https://doi.org/10.1016/J.EST.2023.107132.
[19] A. Pizzolato, A. Sharma, K. Maute, A. Sciacovelli, V. Verda, Design of effective fins for fast PCM melting and solidification in shell-and-tube latent heat thermal energy storage through topology optimization, Appl. Energy 208 (2017) 1–18, https://doi.org/10.1016/j.apenergy.2017.10.050.
[20] B. Golparvar, H. Niazmand, A. Sharafian, H.A. Ahmadian, Optimum fin spacing of finned tube adsorber bed heat exchangers in an exhaust gas-driven adsorption cooling system, Appl. Energy 232 (2018) 504–516, https://doi.org/10.1016/j.apenergy.2018.10.002.
[21] M.S. Fernandes, G.J.V.N. Brites, J.J. Costa, A.R. Gaspar, V.A.F. Costa, Modeling and parametric analysis of an adsorber unit for thermal energy storage, Energy 102 (2016) 83–94.

[22] M.S. Fernandes, A.R. Gaspar, V.A.F. Costa, J.J. Costa, G.J.V.N. Brites, Optimization of a thermal energy storage system provided with an adsorption module – A GenOpt application in a TRNSYS/MATLAB model, Energy Convers Manag 162 (2018) 90–97, https://doi.org/10.1016/J.ENCONMAN.2018.02.027.
[23] A. Pizzolato, Topology Optimization for Energy Problems - Ph.D, Thesis. Politecnico di Torino (2018), https://doi.org/10.1039/B317095K.
[24] Bendsoe M, Sigmund O. Topology optimization: theory, methods, and applications. Springer Berlin Heidelberg; 2004. 10.1007/978-3-662-05086-6.
[25] T. Vaneker, A. Bernard, G. Moroni, I. Gibson, Y. Zhang, Design for additive manufacturing: Framework and methodology, CIRP Ann. 69 (2020) 578–599, https://doi.org/10.1016/j.cirp.2020.05.006.
[26] K. Kant, A. Shukla, D.M.J. Smeulders, C.C.M. Rindt, Performance analysis of a K2CO3-based thermochemical energy storage system using a honeycomb structured heat exchanger, J Energy Storage 38 (2021), 102563, https://doi.org/10.1016/j.est.2021.102563.
[27] C. Lundgaard, K. Engelbrecht, O. Sigmund, A density-based topology optimization methodology for thermal energy storage systems, Struct. Multidiscip. Optim. 60 (2019) 2189–2204, https://doi.org/10.1007/s00158-019-02375-8.
[28] A. Pizzolato, A. Sharma, K. Maute, A. Sciacovelli, V. Verda, Topology optimization for heat transfer enhancement in latent heat thermal energy storage, Int. J. Heat Mass Transf. 113 (2017) 875–888, https://doi.org/10.1016/j.ijheatmasstransfer.2017.05.098.
[29] Y. Tian, X. Liu, Q. Xu, Q. Luo, H. Zheng, C. Song, et al., Bionic topology optimization of fins for rapid latent heat thermal energy storage, Appl. Therm. Eng. 194 (2021), 117104, https://doi.org/10.1016/J.APPLTHERMALENG.2021.117104.
[30] J.T. Chen, B.Q. Xia, C.Y. Zhao, Topology optimization for heat transfer enhancement in thermochemical heat storage. Int, J Heat Mass Transf 154 (2020), https://doi.org/10.1016/j.ijheatmasstransfer.2020.119785.
[31] B. Michel, P. Neveu, N. Mazet, Comparison of closed and open thermochemical processes, for long-term thermal energy storage applications, Energy 72 (2014) 702–716, https://doi.org/10.1016/j.energy.2014.05.097.
[32] J. Stengler, J. Weiss, M. Linder, Analysis of a lab-scale heat transformation demonstrator based on a gas–solid reaction, Energies (2019) 12, https://doi.org/10.3390/en12122234.
[33] J. Stengler, I. Bürger, M. Linder, Performance analysis of a gas-solid thermochemical energy storage using numerical and experimental methods, Int. J. Heat Mass Transf. 167 (2021), 120797, https://doi.org/10.1016/j.ijheatmasstransfer.2020.120797.
[34] M. Richter, E.M. Habermann, E. Siebecke, M. Linder, A systematic screening of salt hydrates as materials for a thermochemical heat transformer, Thermochim Acta 659 (2018) 136–150, https://doi.org/10.1016/J.TCA.2017.06.011.
[35] J.J. Valencia, P.N. Quested, Thermophysical properties, ASM Handb 15 (2008) 468–481, https://doi.org/10.1361/asmhba0005240.
[36] T. Dbouk, A review about the engineering design of optimal heat transfer systems using topology optimization, Appl. Therm. Eng. 112 (2017) 841–854, https://doi.org/10.1016/j.applthermaleng.2016.10.134.
[37] J.H.K. Haertel, K. Engelbrecht, B.S. Lazarov, O. Sigmund, Topology optimization of a pseudo 3D thermofluid heat sink model, Int. J. Heat Mass Transf. 121 (2018) 1073–1088, https://doi.org/10.1016/J.IJHEATMASSTRANSFER.2018.01.078.
[38] J. Alexandersen, N. Aage, C.S. Andreasen, O. Sigmund, Topology optimisation for natural convection problems, Int. J. Numer. Meth. Fluids 76 (2014) 699–721, https://doi.org/10.1002/FLD.3954.
[39] A. Pizzolato, A. Sharma, K. Maute, A. Sciacovelli, V. Verda, Multi-scale topology optimization of multi-material structures with controllable geometric complexity — applications to heat transfer problems, Comput. Methods Appl. Mech. Eng. 357 (2019), 112552, https://doi.org/10.1016/j.cma.2019.07.021.
[40] S. Mauran, H. Lahmidi, V. Goetz, Solar heating and cooling by a thermochemical process. First experiments of a prototype storing 60 kW h by a solid/gas reaction, Sol. Energy 82 (2008) 623–636, https://doi.org/10.1016/j.solener.2008.01.002.
[41] J.E. Edwards, Design and Rating Shell and Tube Heat Exchangers, Chemistations - Technical Report, 2008.
[42] A. Fopah-Lele, C. Rohde, K. Neumann, T. Tietjen, T. Rönnebeck, K.E. N'Tsoukpoe, et al., Lab-scale experiment of a closed thermochemical heat storage system including honeycomb heat exchanger, Energy 114 (2016) 225–238, https://doi.org/10.1016/j.energy.2016.08.009.
[43] B. Michel, N. Mazet, S. Mauran, D. Stitou, J. Xu, Thermochemical process for seasonal storage of solar energy: Characterization and modeling of a high density reactive bed, Energy 47 (2012) 553–563, https://doi.org/10.1016/j.energy.2012.09.029.
[44] G. Balasubramanian, M. Ghommem, M.R. Hajj, W.P. Wong, J.A. Tomlin, I.K. Puri, Modeling of thermochemical energy storage by salt hydrates, Int. J. Heat Mass Transf. 53 (2010) 5700–5706, https://doi.org/10.1016/j.ijheatmasstransfer.2010.08.012.
[45] A. Khawam, D.R. Flanagan, Solid-State Kinetic Models: Basics and Mathematical Fundamentals, J. Phys. Chem. B 110 (2006) 17315–17328, https://doi.org/10.1021/JP062746A.
[46] J. Stengler, I. Bürger, M. Linder, Thermodynamic and kinetic investigations of the SrBr 2 hydration and dehydration reactions for thermochemical energy storage and heat transformation, Appl. Energy 277 (2020), 115432, https://doi.org/10.1016/j.apenergy.2020.115432.
[47] R. Fisher, Y. Ding, A. Sciacovelli, Hydration kinetics of K2CO3, MgCl2 and vermiculite-based composites in view of low-temperature thermochemical energy storage, J Energy Storage (2021) 38, https://doi.org/10.1016/j.est.2021.102561.
[48] Incropera F P, DeWitt D P, Bergman T L, Lavine A S. Fundamentals of heat and mass transfer. 6th ed. 2012.
[49] A. Frazzica, V. Brancato, B. Dawoud, Unified methodology to identify the potential application of seasonal sorption storage technology, Energies (2020) 13, https://doi.org/10.3390/en13051037.
[50] A. Bejan, The constructal law of organization in nature: Tree-shaped flows and body size, J. Exp. Biol. 208 (2005) 1677–1686, https://doi.org/10.1242/jeb.01487.
[51] Kauko H. Industrial Thermal Energy Storage - What Are The Possibilities. n.d.
[52] R.C.R. Amigo, D.S.P.J.L. Paiva, R.W.H.E.C.N. Silva, Topology optimisation of biphasic adsorbent beds for gas storage, Struct. Multidiscip. Optim. (2018:) 2431, https://doi.org/10.1007/s00158-018-2117-x.
[53] Sigmund O, Petersson J. Numerical instabilities in topology optimization: A survey on procedures dealing with checkerboards, mesh-dependencies and local minima. vol. 16. 1998. 10.1007/BF01214002.
[54] Svanberg K. MMA and GCMMA-two methods for nonlinear optimization 2007.
[55] Gothäll H. How to Use Topology Optimization Results as Model Geometries | COMSOL Blog n.d.
[56] Q. Ranjha, N. Vahedi, A. Oztekin, High-temperature thermochemical energy storage – heat transfer enhancements within reaction bed, Appl. Therm. Eng. 163 (2019), 114407, https://doi.org/10.1016/j.applthermaleng.2019.114407.
[57] C. Zhao, Y. Wang, M. Li, W. Du, Heat transfer performance investigation on a finned tube adsorbent bed with a compound parabolic concentrator (CPC) for solar adsorption refrigeration, Appl. Therm. Eng. 152 (2019) 391–401, https://doi.org/10.1016/J.APPLTHERMALENG.2019.02.063.
[58] T. Pham, P. Kwon, S. Foster, Additive manufacturing and topology optimization of magnetic materials for electrical machines—a review, Energies 14 (2021) 1–24, https://doi.org/10.3390/en14020283.
[59] J.R. McDonough, A perspective on the current and future roles of additive manufacturing in process engineering, with an emphasis on heat transfer, Therm Sci Eng Prog 19 (2020), 100594, https://doi.org/10.1016/j.tsep.2020.100594.
[60] B.S. Lazarov, O. Sigmund, K.E. Meyer, J. Alexandersen, Experimental validation of additively manufactured optimized shapes for passive cooling, Appl. Energy 226 (2018) 330–339, https://doi.org/10.1016/J.APENERGY.2018.05.106.
[61] R. Ge, G. Humbert, R. Martinez, M.M. Attallah, A. Sciacovelli, Additive manufacturing of a topology-optimised multi-tube energy storage device: Experimental tests and numerical analysis, Appl. Therm. Eng. 180 (2020), 115878, https://doi.org/10.1016/j.applthermaleng.2020.115878.
[62] M. Johnson, J. Vogel, M. Hempel, B. Hachmann, A. Dengel, Design of high temperature thermal energy storage for high power levels, Sustain. Cities Soc. 35 (2017) 758–763, https://doi.org/10.1016/J.SCS.2017.09.007.
[63] D. Thomas, Costs, benefits, and adoption of additive manufacturing: a supply chain perspective, Int. J. Adv. Manuf. Technol. 85 (2016) 1857–1876, https://doi.org/10.1007/s00170-015-7973-6.
[64] A. Nana, J.C. Cuillière, V. Francois, Automatic reconstruction of beam structures from 3D topology optimization results, Comput. Struct. 189 (2017) 62–82, https://doi.org/10.1016/j.compstruc.2017.04.018.
[65] L. Meng, W. Zhang, D. Quan, G. Shi, L. Tang, Y. Hou, et al., From topology optimization design to additive manufacturing: today's success and tomorrow's roadmap, Arch. Comput. Meth. Eng. 27 (2020) 805–830, https://doi.org/10.1007/s11831-019-09331-1.
[66] E. Borri, G. Zsembinszki, L.F. Cabeza, Recent developments of thermal energy storage applications in the built environment: A bibliometric analysis and systematic review, Appl. Therm. Eng. 189 (2021), 116666, https://doi.org/10.1016/j.applthermaleng.2021.116666.
[67] D. Stitou, N. Mazet, M. Bonnissel, Performance of a high temperature hydrate solid/gas sorption heat pump used as topping cycle for cascaded sorption chillers, Energy 29 (2003) 267–285, https://doi.org/10.1016/j.energy.2003.08.011.
[68] A. Pizzolato, A. Sharma, R. Ge, K. Maute, V. Verda, Maximization of performance in multi-tube latent heat storage – Optimization of fins topology, effect of materials selection and flow arrangements, Energy (2019), https://doi.org/10.1016/j.energy.2019.02.155.